569409
60P

Nanotechnology Infrared Optics for Astronomy Missions

GRANT
TR/IN/89

Grant NAG5-9363

Annual Performance Report No. 2

For the period 1 April 2001 through 31 March 2002

Principal Investigator:

Dr. Howard A. Smith

February 2002

Prepared for
National Aeronautics and Space Administration
Washington D.C.

Smithsonian Institution
Astrophysical Observatory
Cambridge, Massachusetts 02138-1596

The Smithsonian Astrophysical Observatory
is a member of the
Harvard-Smithsonian Center for Astrophysics

The NASA Technical Officer for this grant is Dr. Guy Stringfellow, 076.0, NASA Headquarters, 300 E Street SW, Code SR, Washington DC 20546-0001

Table of Contents

I. Program Objectives 1
II. Overview of Current Status 1
III. Progress Report 2
A. Mesh Modeling 2
B. Filter Fabrication 2
C. Staff and Equipment Changes 3
D. Other Programmatic Matters 3
IV. Program Plans 4
FIGURE CAPTIONS 5
APPENDICES 5

I. Program Objectives

The program "Nanotechnology Infrared Optics for Astronomy Missions" will design and develop new, nanotechnology techniques for infrared optical devices suitable for use in NASA space missions. The proposal combines expertise from the Smithsonian Astrophysical Observatory, the Naval Research Laboratory, the Goddard Space Flight Center, and the Physics Department at the Queen Mary and Westfield College in London, now relocated to the University of Cardiff, Cardiff, Wales. The method uses individually tailored metal grids, and layered stacks of metal mesh grids, both inductive (free-standing) and capacitive (substrate-mounted), to produce various kinds of filters.

The program has the following goals:

1) Model FIR filter properties using electric-circuit analogs, and near-field, EM diffraction calculations;

2) Prototype fabrication of meshes on various substrates, with various materials, and of various dimensions;

3) Test of filter prototypes, and iterate with the modeling programs;

4) Travel to related sites, including trips to Washington, D.C. (location of NRL and GSFC), London (location of QMW), Cardiff, Wales, and Rome (location of ISO PMS project headquarters);

5) Produce ancillary science, including publication of both testing on mesh performance and infrared astronomical science.

II. Overview of Current Status

As of the preparation of this annual report, February 2002, we are pleased to report that very substantial progress has been made. In particular, the original constraints arising from the delayed start-of-funding have now been overcome.

This proposal had been originally submitted in response to NASA NRA-96-OSS-07, in June 1996, with positive notification of the review coming in April 1997. However, because of budget constraints at NASA, the PI agreed to accept a delay in funding. This delay was extended at the request of NASA several times. Grant notification finally arrived on 21 April 2000, with an effective start date of 1 April 2000. The very long delay between original submission and start of the program (just three months shy of four years) presented several logistical difficulties which were discussed and agreed to by NASA and the PI as being unfortunate but acceptable. These included the fact that key personnel – in particular Dr. John Miles, who had been the post-doc running the program, and Mr. Brian Hicks, the project technician – both had to accept other positions in the interim. As planned and agreed upon, notification of the award initiated a three-part process of regrouping, as described in earlier reports, and which, as of January 2001, were well underway.

In particular:

- During this past year the project has hired an outstanding physicist to lead the technical development, Dr. Ken Stewart. He has now taken up residence at the Naval Research Laboratory.

- We have leverage funds to purchase Bruker IFS66v Mid and Far Infrared Fourier Transform Spectrometer, which will be used for filter calibrations.

- We have continued to work on modeling of the filters, published several papers, and converged on a reasonable representation.

- We have succeeded in fabricating a resonant mesh grid on polyimide substrate, measured its per-

formance, and found it is in fair agreement with the theoretical model.

- Project collaborators Dr. P. A. R. Ade and his group have completed the move of their entire operations (including ~38 people!) from their location at Queen Mary and Westfield College, London, to the University of Cardiff, Cardiff, Wales. We look forward to renewing interactions with them again.

III. Progress Report

We take note that to date the program budget received cuts from NASA of $27,512 from the original budget request. This is not an insignificant amount, and has meant both moving more slowly, and eliminating some planned tasks. If possible, restoration of some or all of these funds in the out year would be most desirable; at the least we hope there will be no further reductions of the planned budget.

A. Mesh Modeling

We have been using the "Microstripes" code (Flomerics, Inc.) to perform full, near and far field diffraction modeling of metal mesh performance on substrates. Our "Miles Code" software, which approximates the full calculation in a quick, GUI-based window, is useful as an iterative device by adjusting the input parameters (index of refraction, thickness, etc.) to provide agreement with the full calculation. However, despite the somewhat extravagant claims by the Microstripes manufacturer, this code is also not perfect because numerous free parameters must be set. Key among these, as identified in our earlier papers and proposal documents, is the high frequency (i.e., far IR) character of the real and imaginary parts of the index of refraction of the metal mesh, the high frequency character of the real and imaginary parts of the index of refraction of the substrate, and the character of the interface between the mesh and the substrate material, and in particular the suppression (or possible enhancement) of surface effects at the interface. Figure 1 shows the results of a Microstripes model calculation of a resonant metal grid on polyimide with parameters g=21, a=4.2, and b=1.575. (See Figure 2 for a review of the definition of these terms.) Figure 3 shows a Miles Code calculation of the same geometry, but with the input parameters adjusted to compensate for the approximations made in this code. This filter was designed at the request of a SOFIA (Stratospheric Observatory for Infrared Astronomy) instrument team for potential use there. The model filter, a single element resonant structure on polyimide, has a resolving power of 5.8, and a central wavelength at 262 cm^-1. The design would be an extremely valuable component to the SOFIA instrument if it can be fabricated with the high transmission projected by the calculation. This, however, is predicated on understanding the actual performance of the material at both room and cryogenic temperatures.

B. Filter Fabrication

We fabricated a resonant, inductive metal mesh on polyimide. The polyimide substrate material was provided by Dr. Christine Allen of NASA's Goddard Space Flight Center (Code 553). We then tested the performance of the filter using the NASA GSFC FTS, at both room temperature and 4.5K. Figures 4a and 4b show the results from measurements of two of the samples – one wrinkled, and one smooth.

The results from the measurements were in very good agreement with the modeling. The model predicted a transmission peak at 262 cm^-1, with a FWHM of 45 cm^-1. The measurements gave a performance peak transmission of 0.64 at 285 cm^-1, with a FWHM of 40cm^-1. The disagreement in peak transmission frequency is 13.4%, and the disagreement in FWHM is 12%. Both of these results are deemed acceptable, given the uncertainties in the physical parameters of the mesh and its substrate.

C. Staff and Equipment Changes

Dr. Ken Stewart of the NASA Goddard Space Flight Center has also joined the team, and has been hired by the Naval Research Laboratory's Remote Sensing Division. He has in this past year assumed his NRL position. This will enable him to work more fully on the mesh effort (although the program funding is not adequate to cover his full salary and he works on other NRL projects as well). Dr. Stewart had worked with Mr. Hicks and our group in past years testing the metal meshes in the laboratory. The cryogenic Fourier Transform Spectrometer at GSFC, under his supervision, is an outstanding measurement tool, capable of the 1% or better calibration deemed essential for our samples.

Dr. K. Moller of the Department of Physics and Electronic Imaging of the New Jersey Institute of Technology is participating with the team on modeling projects. Dr. Moller is a senior scientist, and has worked on meshes for over 30 years. This project helps to support his involvement, through a subcontract with NRL.

Drs. Stewart and Moller are experts at using the "Microstripes" Code for metal mesh modeling. Unlike the analytic code which the program uses for quick analyses, the Microstripes code is a full-up diffraction and near-field calculation taking several hours of running time per sample.

Dr. Christine Allen and Dr. Lee Feinberg of the NASA Goddard Space Flight Center make thin SiN and polyimide films in their facility, and have provided a sample to us for testing in warm and cryogenic conditions.

Not least, project collaborators Dr. P. A. R. Ade and his group have completed the move of their entire operations from Queen Mary and Westfield College to the University of Cardiff, in Cardiff, Wales.

The Bruker IFS66v Mid and Far Infrared Fourier Transform Spectrometer will be a key part of this program. Leveraging Naval Research Laboratory funds, our Co-I Dr. J. Fischer was able to purchase this new equipment. In the past our measurements were done at the Goddard Space Flight Center and its Bomem FTS; the new instrument is significantly easier to use, and under the skill of Dr. Stewart should give us routinely, and with greater ease and flexibility, the precision we need at the cryogenic temperatures. The instrument has not yet been set up, and this is one of the key goals of the next year's work. Appendix B provides some background information on the FTS, as taken from the Bruker website.

D. Other Programmatic Matters

During this past year we have held a series of team meetings. While Dr. Stewart was still at Goddard the meetings tended to be held there, but, as noted, he has now moved to NRL and most meetings will be located there. As projected in last year's planning document, we also traveled to a meeting with our collaborator at Queen Mary and Westfield College in London. This group has now made a major move to the University of Cardiff, in Cardiff, Wales. During the coming year we anticipate at least one trip to the new laboratory location to review progress and compare notes. It is a program goal to obtain some independent confirmation of the filter performance by making measurements at the UC laboratory. Also as anticipated, we completed travel to the Istituto Fisica Spaziale Interplanetario laboratory in Rome, Italy, where we worked with team collaborators on the FIR spectra obtained with the Infrared Space Observatory's Long Wavelength Spectrometer. This Italian group is the headquarters for the ISO/LWS data on main sequence stars. This group is also active in the development of the Herschel spacecraft.

The following publications have been prepared during this interval since 2000, including, as projected in the program plan, ancillary science publications:

"Inductive Cross Shaped Metal Meshes and Dielectrics," by Moller, Sternberg, Grebel, and Stewart (submitted to Infrared Physics).

"Shock excited far-infrared molecular emission around T Tau," Spinoglio, L., Giannini, T., Nisini, B., van den Ancker, M. E., Caux, E., Di Giorgio, A. M., Lorenzetti, D., Palla, F., Pezzuto, S., Saraceno, P., Smith, H. A., and White, G. J., *Astr. Ap.*, **353**, 1055, 2000.

"Large Proper-Motion Infrared [FE II] Emission-Line Features in GGD 37," Raines, S.N., Watson, D., Pipher, J., Forrest, W., Greenhouse, M., Satyapal, S., Woodward, C., Smith, H.A., Fischer, J., Goetz, J., and Frank, A., *Ap.J.*, **528**, 115, 2000.

"The ISO spectroscopic view of the HH 24-26 region," Benedettini, M., Giannini, T., Nisini, B., Tommasi, E., Lorenzetti, D., Di Giorgio, A. M., Saraceno, P., Smith, H. A., White, G. J., *A&A*, **359**, 148, 2000.

"Looking at the photon-dominated region in NGC 2024 through FIR line emission," Giannini, T., Nisini, B., Lorenzetti, D., Di Giorgio, A. M., Spinoglio, L., Benedettini, M., Saraceno, P., Smith, H. A., White, G. J., *A&A*, **358**, 310, 2000.

"Far infrared spectroscopy of FU Ori objects. ISO-LWS observations," Lorenzetti, D., Giannini, T., Nisini, B., Benedettini, M., Creech-Eakman, M., Blake, G. A., van Dishoeck, E. F., Cohen, M., Liseau, R., Molinari, S., Pezzuto, S., Saraceno, P., Smith, H. A., Spinoglio, L., White, G. J., *A&A*, **357**, 1035, 2000.

"ISO-LWS spectroscopy of Centaurus A: extended star formation Unger," S. J., Clegg, P. E., Stacey, G. J., Cox, P., Fischer, J., Greenhouse, M., Lord, S. D., Luhman, M. L., Satyapal, S., Smith, H. A., Spinoglio, L., Wolfire, M., *A&A*, **355**, 885, 2000.

"ISO spectroscopy of Seyfert galaxies: fine structure line detections in seven galaxies," Spinoglio, L., Benedettini, M., de Troia, G., Malkan, M. A., Clegg, P. E., Fischer, J., Greenhouse, M., Satyapal, S., Smith, H. A., Stacey, G. J., Unger, S. J., *ISO Beyond The Peaks: The 2nd ISO Workshop On Analytical Spectroscopy*. Eds. Salama, Kessler, Leech, and Schulz. ESA-SP 456, p. 79, 2000.

"Atomic and molecular cooling in pre-main sequence objects: the ISO view," Saraceno, P., Benedettini, M., de Troia, G., di Giorgio, A. M., Giannini, T., Lorenzetti, D., Molinari, S., Nisini, B., Pezzuto, S., Smith, H. A., Spinoglio, L., White, G. J., *ISO Beyond The Peaks: The 2nd ISO Workshop On Analytical Spectroscopy*. Eds. Salama, Kessler, Leech, and Schulz. ESA-SP 456, p. 75, 2000.

"Challenges in Affecting US Attitudes Towards Space Science," Smith, H.A., in *Advances in Space Research*, COSPAR-2000 Warsaw Symposium "The Public Understanding of Space Science," Elsevier, Oxford, UK, 2000.

"An Infrared Study of the L1551 Star Formation Region," White, G., Liseau, R., Men'shchikov, A., Justtanont, K., Nisini, B., Benedettini, M., Caux, E., Correia, J., Giannini, T., Kaufman, M., Lorenzetti, D., Molinari, S., Saraceno, P., Smith, H.A., Spinoglio, L., and Tommasi, E., *A&A*, in press, 2000.

"Do Mergers Stop Monsters?" Kewley, L., Dopita, M., and Smith, H.A., *B.A.A.S.*, 2002.

IV. Program Plans

Now that we have successfully brought our staff to its full complement, acquired the necessary instrumentation, and successfully modeled the filters, our goals in the next period will be to fabricate a set of filters under varying conditions, and determine the best process steps in terms of both product yield and product performance.

- Bring the Bruker FTS on line, and get some experience using it.

- Work with NRL and GSFC to produce a set of polyimide-based resonant inductive metal mesh grid filters under varying fabrication conditions.
- Test the above set of filters, and evaluate optimum technologies.
- Iterate one time towards producing a set of mesh filters to be used in a stack.
- Assemble 2 or more of the iterated mesh filters into a composite filter with narrower bandwidth. This is certainly the key aspect of the entire effort. Figure 3c shows the Miles Code calculation of the mesh filter transmission from a series of two stacked filters; these have NOT yet been modeled with the Microstripes code. The transmission FWHM narrows considerably (as expected).

The fabrication challenge will be to keep the peak transmission at a value of >=50% even with the two filters. There are several routes we might take to achieve this goal:

- use thinner layers of polyimide
- substitute other substrate materials for polyimide
- attempt free-standing layering (i.e., without any polyimide at all)

In addition to controlling the absorption, we will need to control the stacking thickness (here designed as 5.0 microns) to ± 30%. Figure 3d shows the effect of stacking 3 filters; this is shown just for curiosity's sake – a more likely fabrication scenario would be to layer filters of different characteristics.

FIGURE CAPTIONS

Figure 1: Microstripes model of a resonant grid filter on a polyimide substrate.

Figure 2: Metal mesh geometry – review of definition of terms.

Figure 3a,b,c,d: Miles Code calculations of filter performance, based on the grid design above (Figure 1). Figure 3a shows the performance with a dummy index of refraction of 0.7; this is used to duplicate the position of the transmission peak. Figure 3b shows that a more physical index can be used if the geometrical parameter g is reduced by about 10%, with good agreement with the Microstripes Code. Figure 3c shows the transmission of a series of two stacked filters; these have NOT yet been modeled with the Microstripes code. Figure 3d shows the effect of stacking 3 filters. The transmission FWHM narrows considerably (as expected).

Figure 4a/b: Room temperature and 4.5K transmission of a resonant inductive metal mesh grid filter on a thin (~2 micron) sample of polyimide provided by Dr. Christine Allen. Two different samples with nominally the same parameters are shown.

Figure 5: Transmission of cold sample of polyimide 2 microns thick.

APPENDICES

APPENDIX A: Preprint: "Inductive Cross Shaped Metal Meshes and Dielectrics," by Moller, Sternberg, Grebel, and Stewart.

APPENDIX B: Some specifications of the newly acquired Bruker Far IR FTS (taken from the Bruker website).

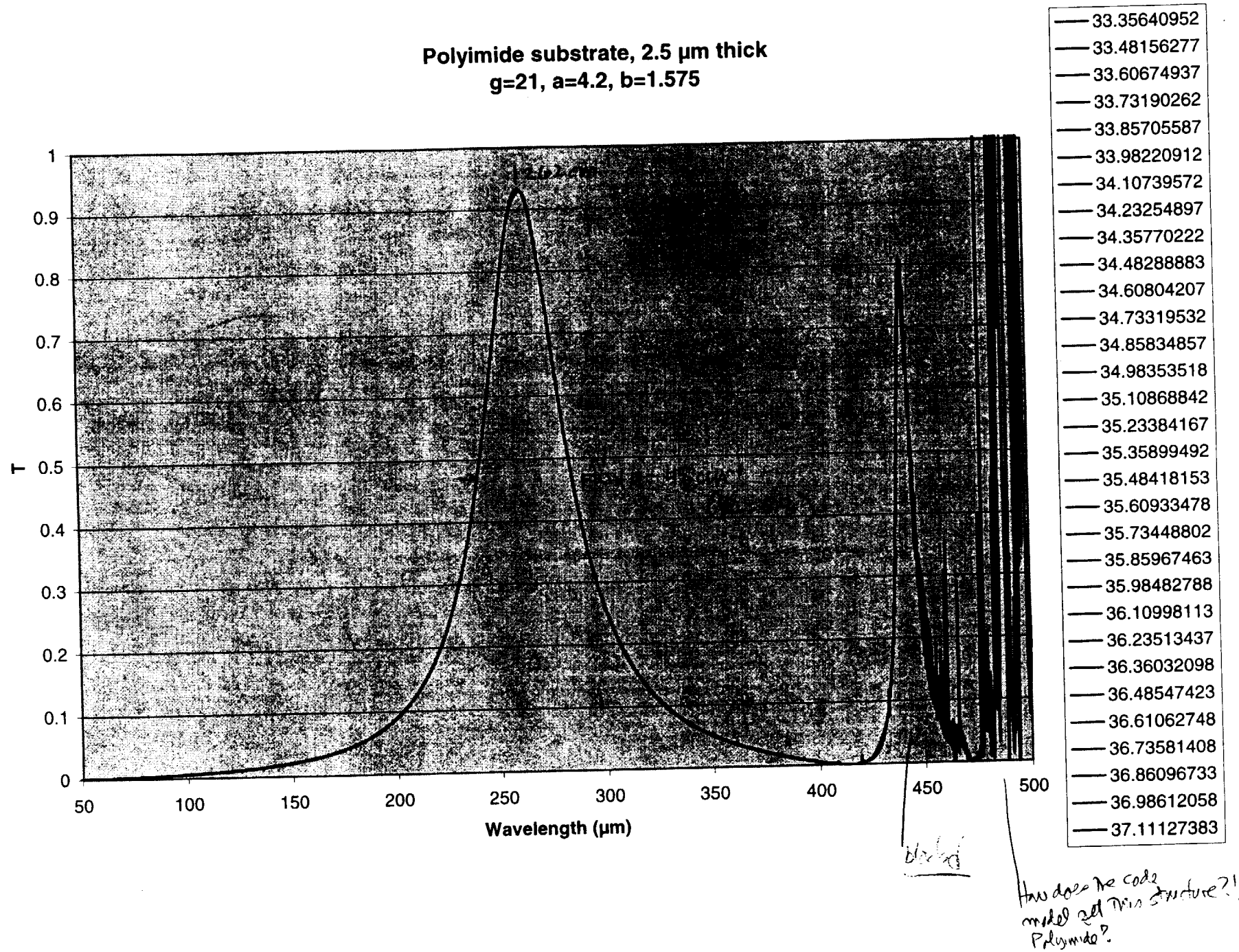

Figure 1

How does he code model 2d Thin structure?! Polyimide?

ken-forecast_pi21.xls MAIN FILTER

Resonant Grid Geometry:

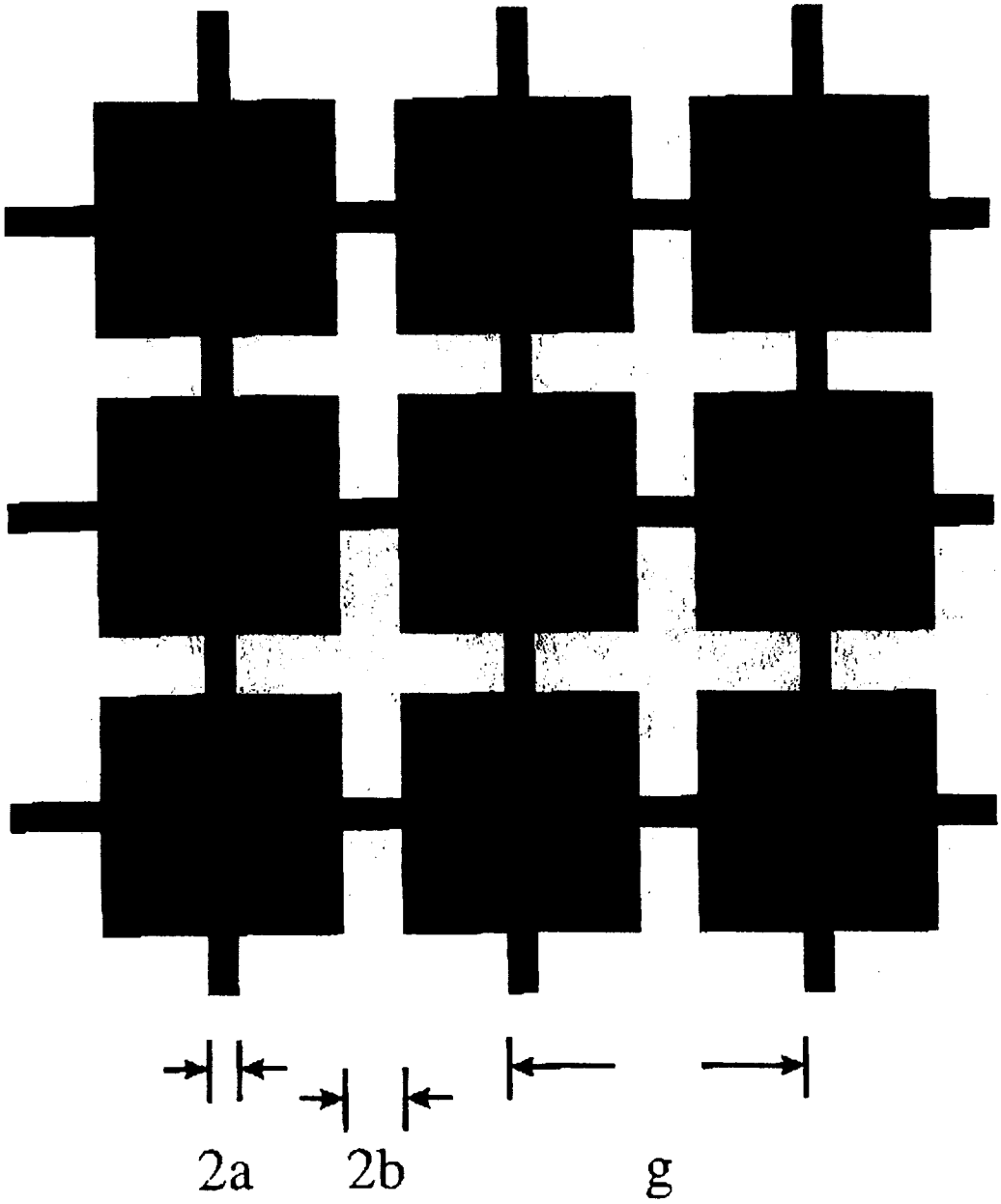

Suggested geometries:

1. R12.5 with g = 12.5μ , a/g = 0.06 , b/g = 0.09;
2. R20 with g = 20μ , a/g = 0.06 , b/g = 0.09;
3. R70 with g = 70μ , a/g = 0.06 , b/g = 0.09;
4. R12.5 with g = 12.5μ , a/g = 0.06 , b/g = 0.125.

Figure 2

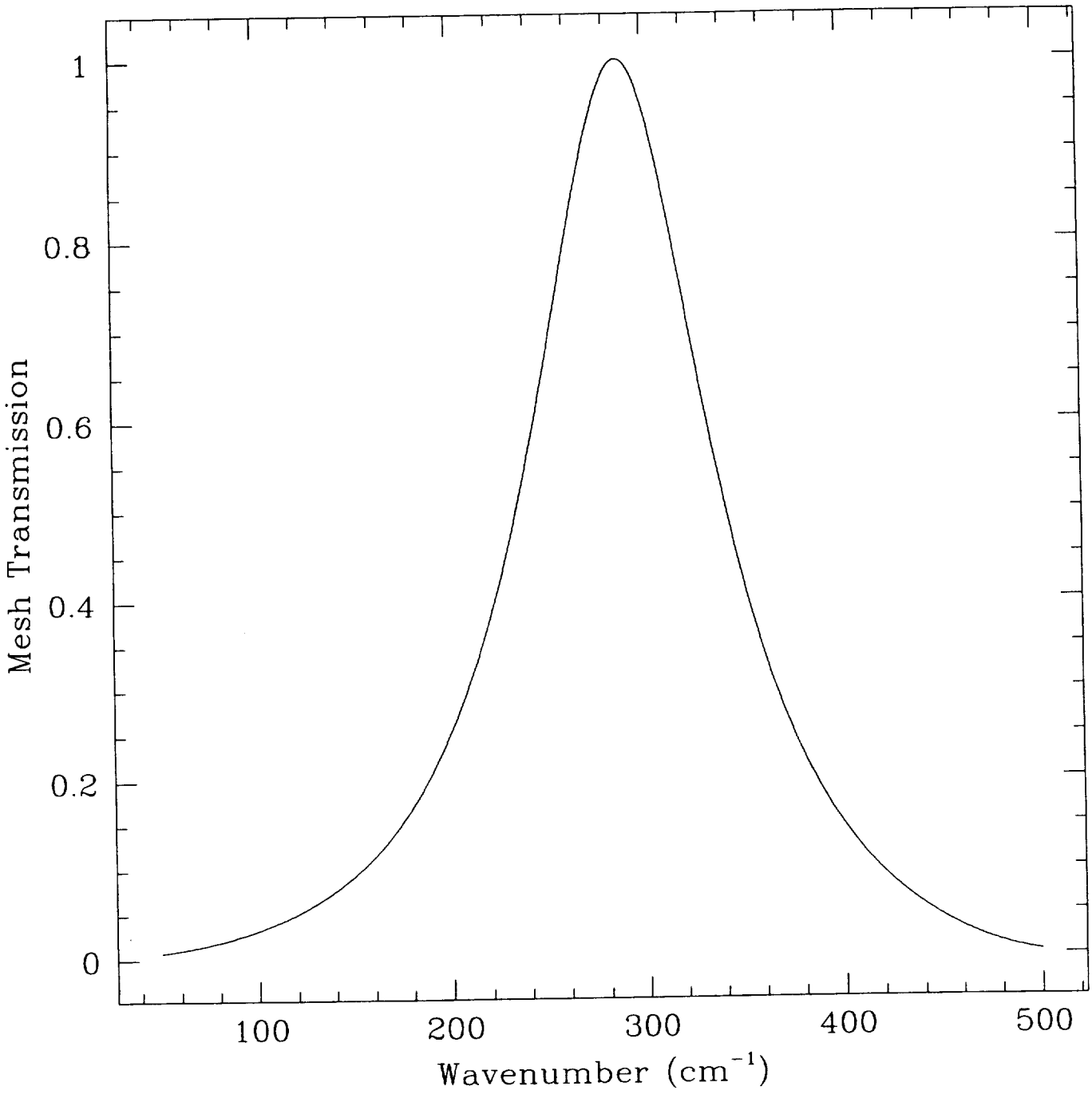

Miles Code
R
g=22
a= 4.4
b= 1.650
t= 0.1
i = 0.70

Figure 3a

Miles Code

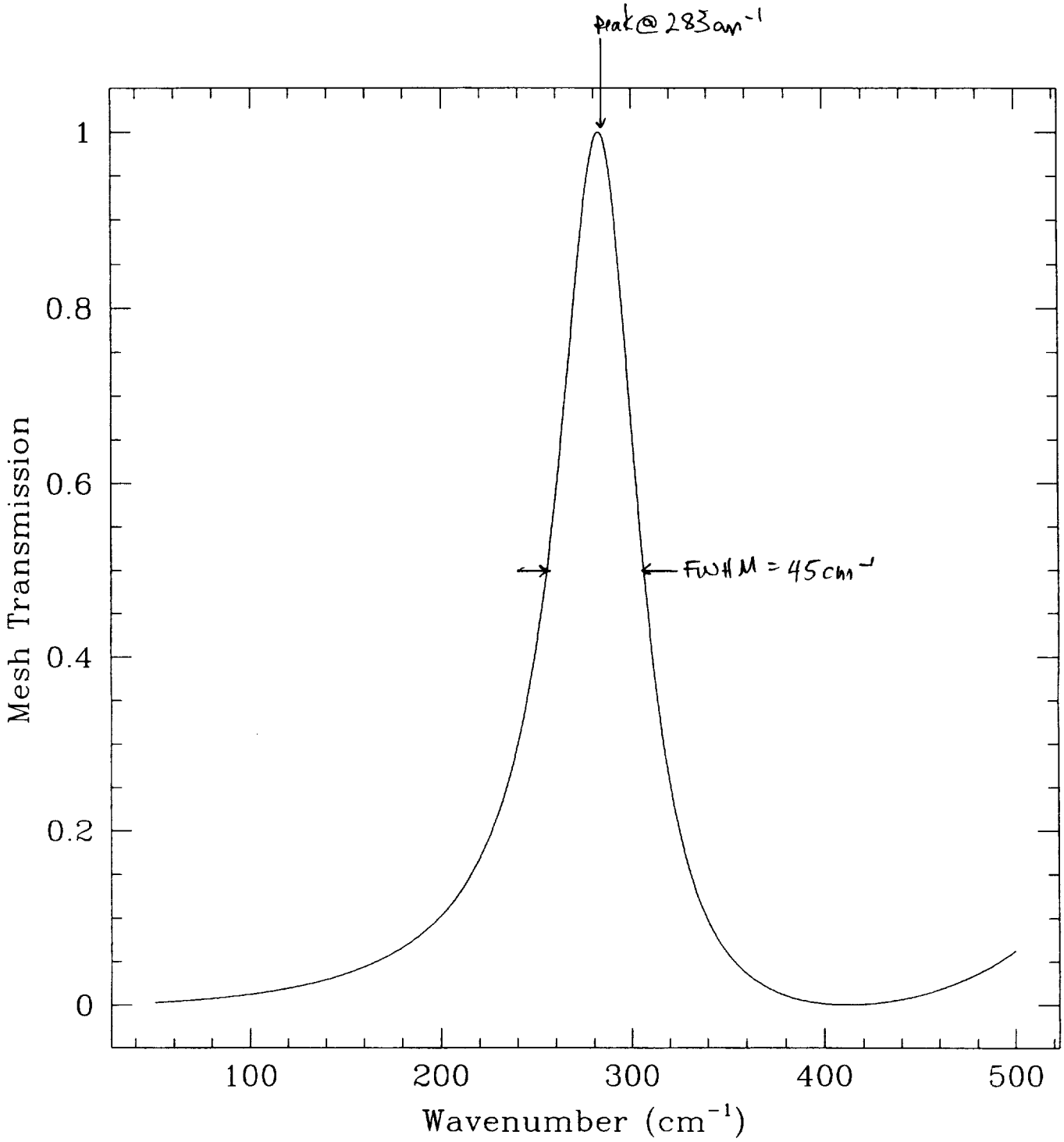

Figure 3b

Miles Code

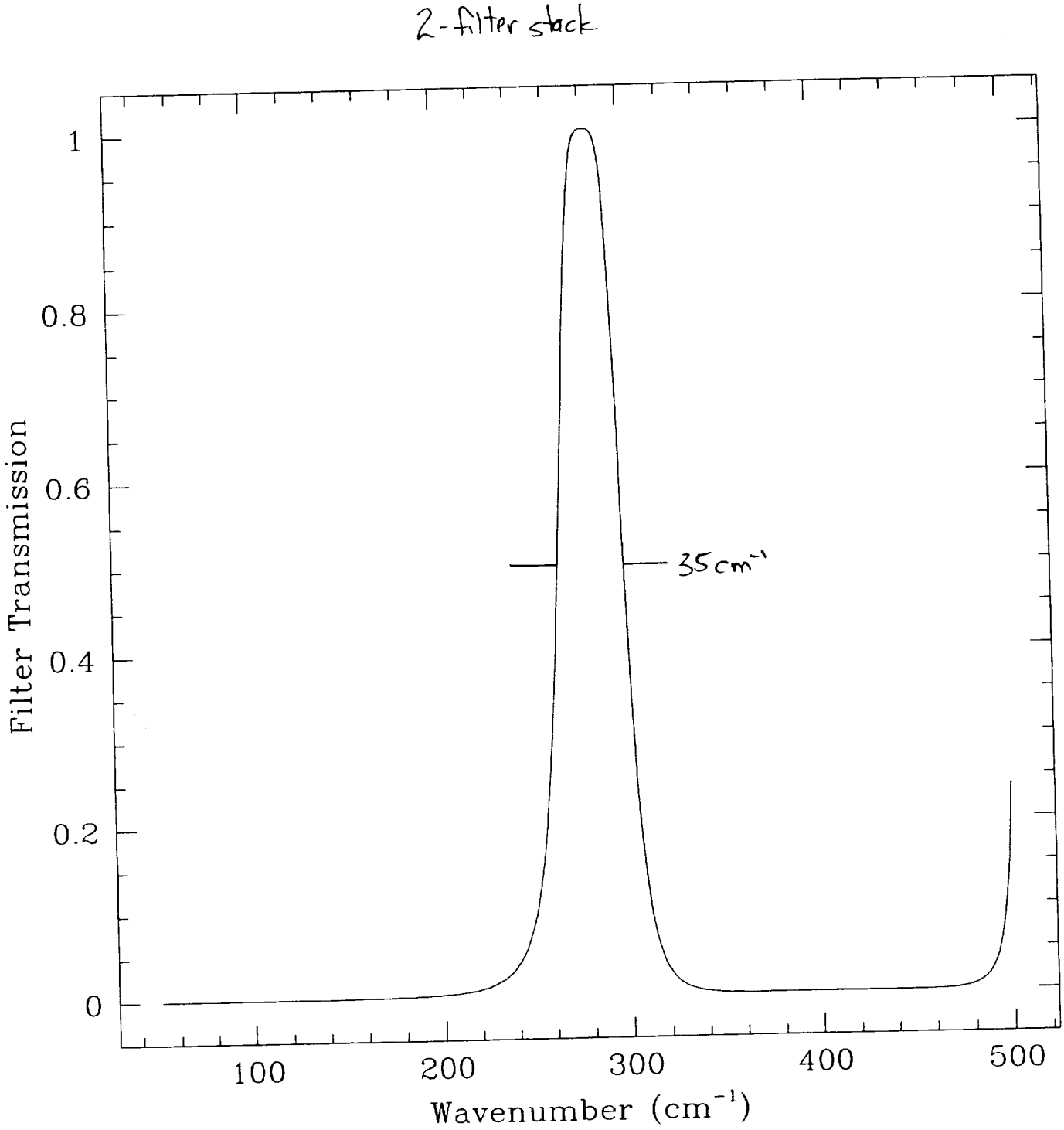

R
g = 18.6
a = 4.4
b = 1.65
t = 0.1
i = 1.50
s = 5.0μm

Figure 3c

Miles Code

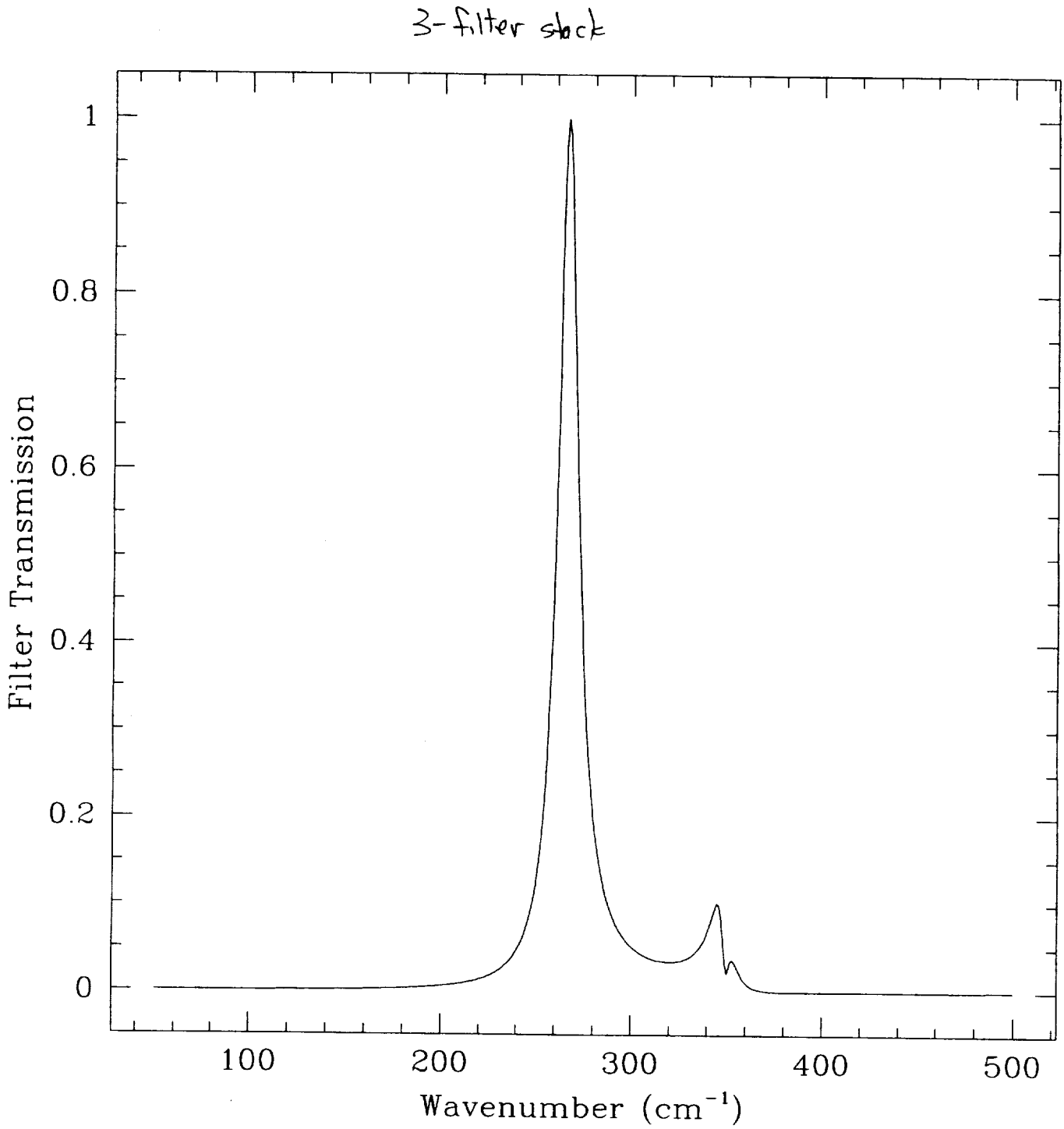

R
g = 18.6
a = 4.4
b = 1.65
t = 0.1
i = 1.50
s = 0.4μm

Figure 3d

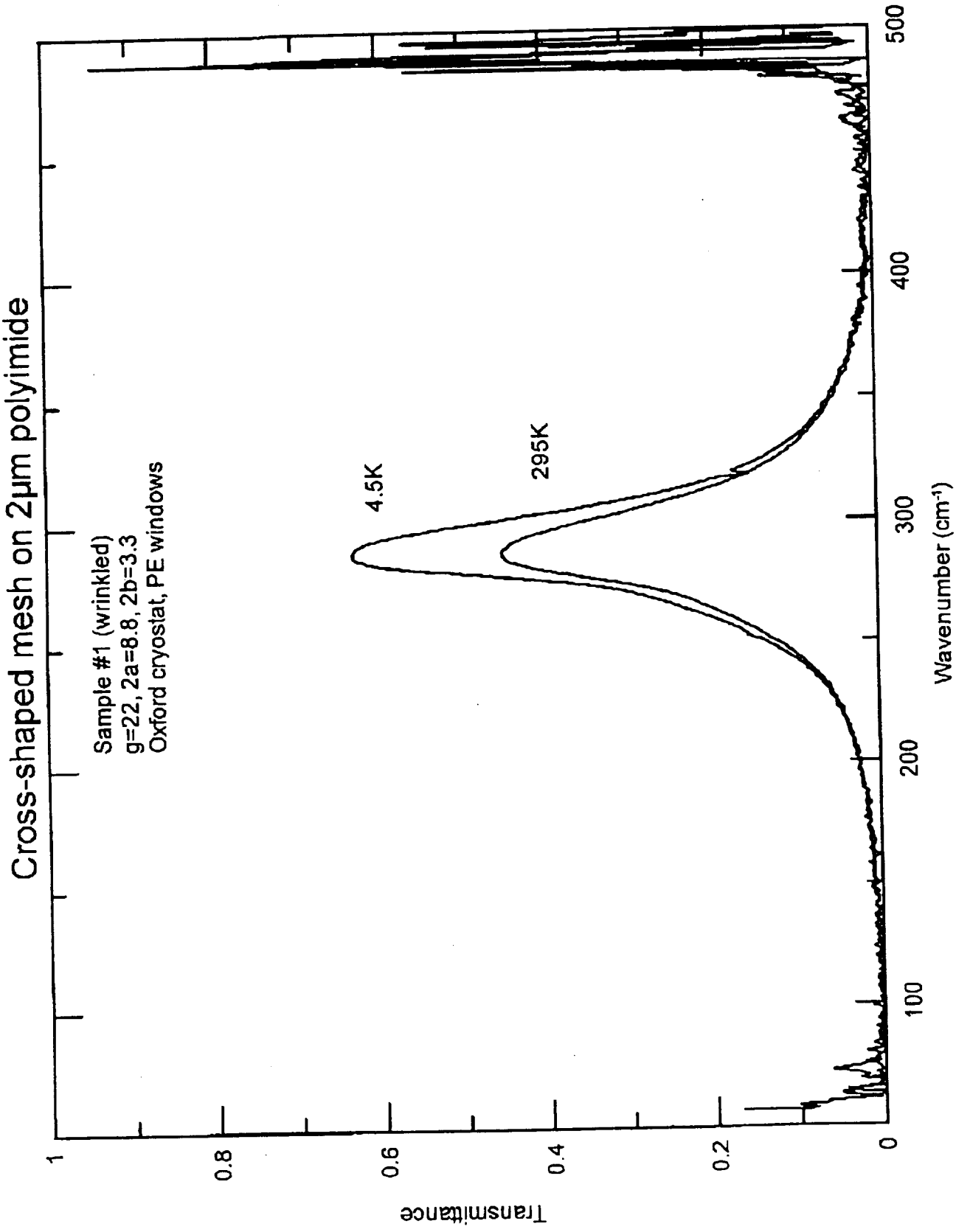
Cross-shaped mesh on 2μm polyimide
Sample #1 (wrinkled)
g=22, 2a=8.8, 2b=3.3
Oxford cryostat, PE windows
4.5K
295K
Transmittance
Wavenumber (cm-1)
0
0.2
0.4
0.6
0.8
1
100
200
300
400
500

Figure 4a

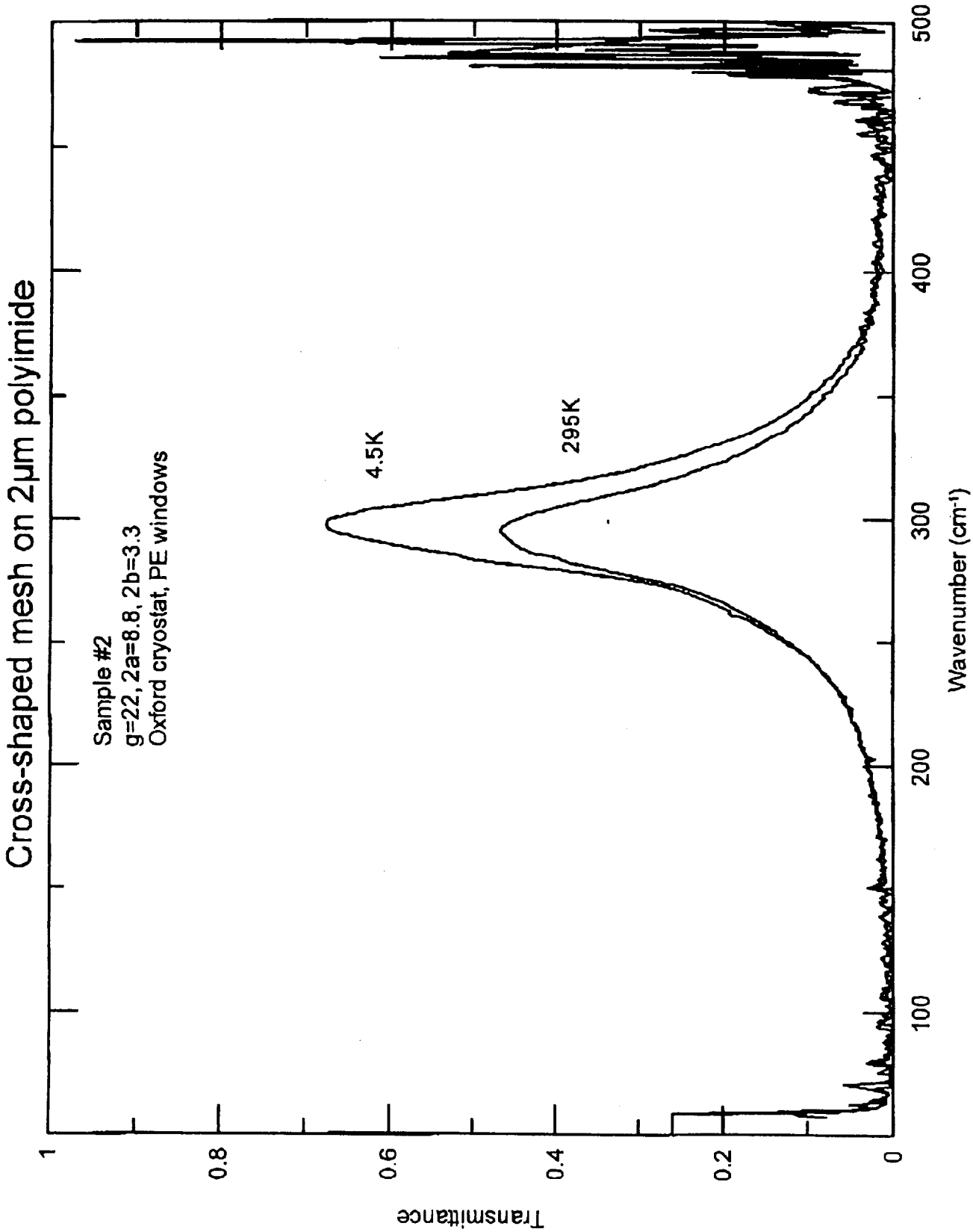
Cross-shaped mesh on 2μm polyimide
Sample #2
g=22, 2a=8.8, 2b=3.3
Oxford cryostat, PE windows
4.5K
295K
Transmittance
Wavenumber (cm-1)
0
0.2
0.4
0.6
0.8
1
100
200
300
400
500

Figure 4b

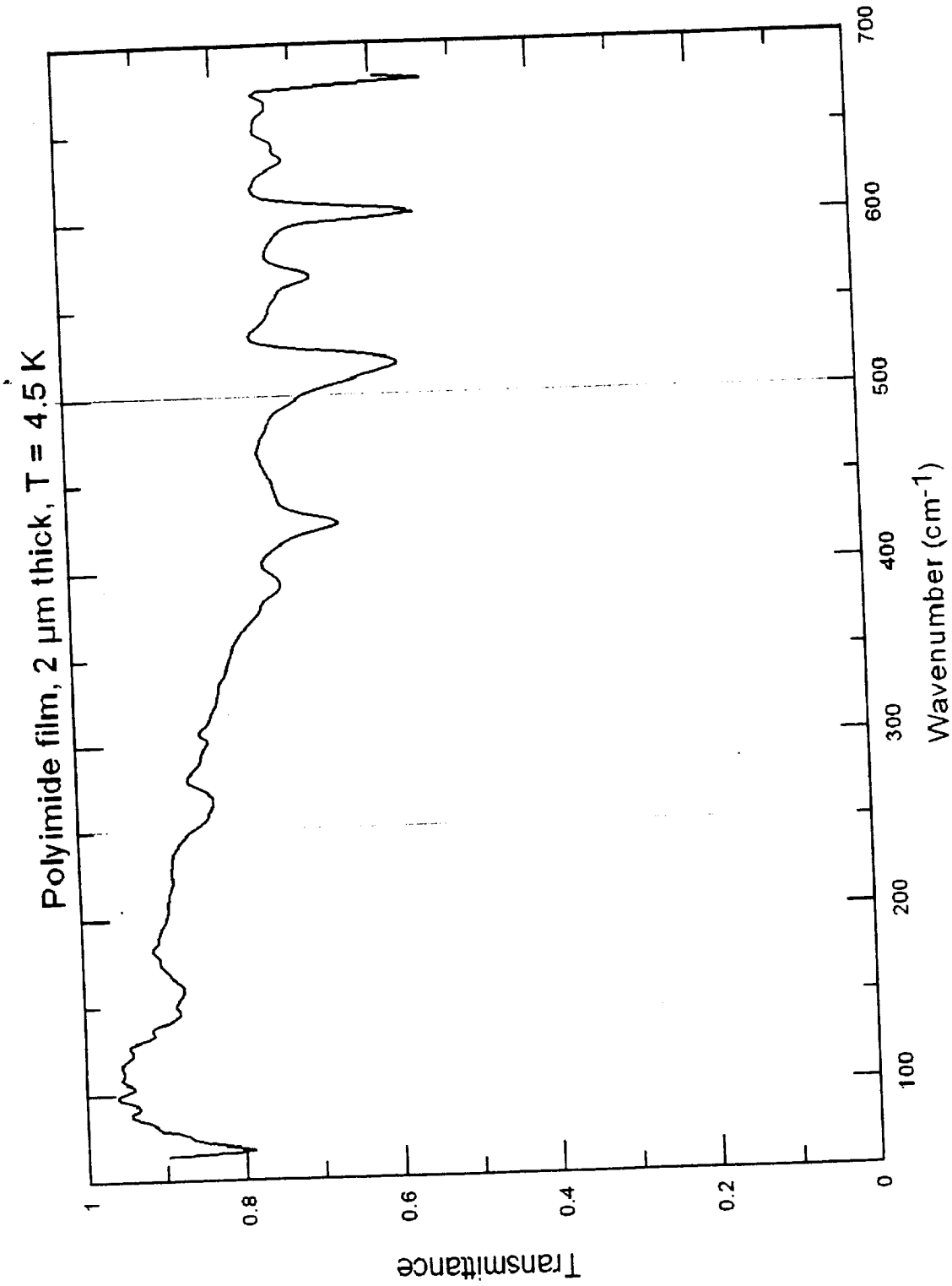
Polyimide film, 2 μm thick, T = 4.5 K
Transmittance
1
0.8
0.6
0.4
0.2
0
100
200
300
400
500
600
700
Wavenumber (cm-1)

Figure 5

INDUCTIVE CROSS SHAPED METAL MESHES AND DIELECTRICS.

K. D. Möller and O. Sternberg
Department of Physics and the Electronic Imaging Center, New Jersey Institute of Technology, Newark NJ 07102

and

H. Grebel
Electronic Imaging Center and the Electrical Engineering Department, New Jersey Institute of Technology, Newark NJ 07102.

and

K. P. Stewart,
Goddard Space Flight Center, Greenbelt MD 20771.

Abstract

Calculations of resonance wavelength and bandwidth of inductive cross shaped metal meshes, free standing or supported by dielectric layers, have been performed using the Micro-Stripes program. The dependence of the shift of the resonance wavelength on the thickness and refractive index of dielectric layers has been described by a "pair of coupled surface plasmons". The approximate width of the surface plasmons in direction normal to the surface has been obtained. The transmittance of two mesh filters with dielectric layers are calculated for specific alignment of the crosses of one mesh with respect to the other. A coupled oscillator model has been used for discussion of the interaction of the resonance wavelengths of the two meshes with one another and with the Fabry-Perot modes. Design procedures for two mesh filters are given.

1. Introduction

Electroformed metal meshes have been used in the 60s by Ulrich[1] as Fabry-Perot reflectors in the far infrared. These square shaped metal meshes, called by Ulrich[2] "inductive" grids, showed high reflectivity and low losses over a large spectral region and were used in the long wavelength region as band pass filters. The inverse structure, first published by Ressler and Möller[3], were called "capacitive" grids" and used as low pass filters.
Ulrich[4] introduced a combination pattern of grids and squares for the manufacturing of cross shaped grids and Chase and Joseph[5] studied in detail the resonance wavelength and the bandwidth. Two patterns are shown in Fig. 1: a mesh with the shape of crosses shown

in Fig.1a has a large bandwidth of about 50% to 60%, while a mesh as shown in Fig.1b has a smaller bandwidth of about 20%.
Ulrich[2] developed transmission line theory for monitoring multiple mesh filters and introduced the "damped oscillator" model. Timusk and Richards[6], following Ref.7, used cascading matrices for transmission line calculations of multi-layer capacitive meshes on dielectric substrates.
Cross shaped metal meshes on Silicon substrate have been investigated experimentally by Hicks[8] and Möller et al[9] and the Micro-Stripes program[10] was successfully used to reproduce the experimental data.
We have used in a preceding paper[11] the Micro-Stripes program to calculate the near field effect of multi-layer cross shaped free standing metal meshes. In this paper we will use the Micro-Stripes program to study the resonance wavelength and bandwidth of a single metal mesh on dielectric layers. The input data are the geometrical parameters of the cross, the surface impedance of the metal mesh and the refractive index and thickness of the dielectric layers. In contrast, transmission line theory uses the resonance wavelength and bandwidth as input parameters for transmittance calculations of a single mesh.
The Micro-Stripes program calculates the transmittance of two metal meshes separated by a dielectric spacer, but gives very different results depending on whether the two meshes are lined up, or whether the second mesh is displaced a distance g/2, in the plane of the mesh, with respect to the first. Because of boundary condition symmetry requirements, these two configurations are the only ones that Micro-Stripes is able to calculate.
Transmission line theory may be used to calculate the transmittance of two metal meshes for a non-aligned configuration as one has for experimental two mesh filters. However, using as input data the Micro-Stripes results for a single mesh, the transmission line calculations do not account for the shift of the resonance wavelength of the meshes depending on the thickness of thin dielectric layers.

2. Transmission line theory.

In analogy to microwave theory, Ulrich developed transmission line theory for the calculation of reflectance and transmittance of metal meshes[2]. The theory uses geometrical and electrical parameters for the description of optical properties. A short description is given in Ref.12.
The theory is semi-empirical and in its original formulation employs only three parameters related to a single mesh. These parameters are the resonance frequency ω_o, the bandwidth A1 and the loss parameter a1. The theory is limited to the wavelength region larger than the periodicity constant.
In the following we will list the essential formulas for the oscillators and the cascading matrices and the expressions for the transmitted and reflected intensities.

A. Oscillator Expressions.

We consider only thin grids, and the shunt impedance of inductive grids is taken as

$$Y(\lambda) = 1/[a1 - i(\omega\, A1)/\Omega(\lambda)] \qquad (1)$$

where $\omega = \omega_o\sqrt{2}/(n_1^2 + n_2^2)$ (2)

and $$\Omega(\lambda) = g/\lambda\omega - \lambda\omega/g. \qquad (3)$$

The resonance frequency of the mesh is ω_o and the corresponding wavelength may be obtained form an empirical formula for thin inductive cross shaped grids[5]. The loss parameter a1 is taken as 0.001, see Ref.13. The bandwidth parameter A1 may be calculated using the Micro-Stripes program or chosen from empirical data.

B. Cascading matrices

The waves on the left side of the impedance Y, see Fig.2, are related to the waves on the right side by a matrix M as

$$\begin{aligned} b_1 &= m_{11}\, a_2 + m_{12}\, b_2 \\ a_1 &= m_{21}\, a_2 + m_{22}\, b_2 \end{aligned} \qquad (4)$$

For $a_2 = 0$ one has for the ratio of reflected wave b_1 to incident wave a_1

$$b_1/a_1 = m_{12}/m_{22} \qquad (5)$$

and for the transmitted wave

$$b_2/a_1 = 1/m_{22}. \qquad (6)$$

The cascading matrix M1 describes the impedance at the interface of a metal mesh with dielectrics of refractive index n_1 on the left and n_2 on the right and is given as

$$\begin{aligned} m1_{11} &= [-Y + (n_1 + n_2)]/2n_1 & m1_{12} &= [-Y + (n_1 - n_2)]/2n_1 \\ m1_{21} &= [Y + (n_1 - n_2)]/2n_1 & m1_{22} &= [Y + (n_1 + n_2)]/2n_1 \end{aligned} \qquad (7)$$

The cascading matrix M2 describes the impedance at the interface of a dielectric with refractive index n_1 on the left and n_2 on the right and is given as

$$m2_{11} = (n_1 + n_2)/2n_1 \qquad m2_{12} = (n_1 - n_2)/2n_1$$
$$m2_{21} = (n_1 - n_2)/2n_1 \qquad m2_{22} = (n_1 + n_2)/2n_1 \tag{8}$$

The matrix M3 describes a transmission line without losses of length d in the medium with refractive index n.

$$m3_{11} = \exp(-i2\pi dn)/\lambda \qquad m3_{12} = 0$$
$$m3_{21} = 0 \qquad m3_{22} = \exp(i2\pi dn)/\lambda \tag{9}$$

Losses may be included in M1 to M3 by using a complex refractive index.
A combination of several matrices of the type M1, M2, and M3 will now be used for the calculation of the transmittance of various combinations of metal meshes with dielectric layers. Two metal meshes with a dielectric spacer will be described by the matrix product Mb =M1M3M1, and two metal meshes embedded in a dielectric by a seven matrix product Mf = M2M3M1M3M1M3M2. The refractive indices have to be specified appropriately in each matrix, and also the thickness in M3 type matrices.

3. Calculations based on Electromagnetic theory.

Many authors have used electromagnetic wave theory for the calculation of the transmittance of metal meshes. We like to cite only a few. Dawes et al[14] studied capacitive grids on substrates of various refractive indices and compared with transmission line calculations and experimental observations. Compton et al[15] studied free standing cross shaped inductive grids and predicted the "thickness" peaks. Porterfield et al[16] used Fourier expansions and the commercially available HFSS program[17] to study thin cross shaped grids.
The Micro-Stripes program has been used successfully by Möller et al.[9] to reproduce the transmittance of thin inductive and capacitive metal meshes on thick Silicon substrates. The agreement with the experimental data are excellent. Therefore we think that one can consider the Micro-Stripes program calculations equivalent to "experimental results".

4. Free standing single metal meshes.

A. Resonance wavelength.

The Micro-Stripes program needs as input data the geometrical parameters of the cross, the thickness of the metal mesh and the surface impedance. From the calculated transmittance one obtains the resonance wavelength and the bandwidth. The losses may

be determined from the choice of the surface impedance. We have calculated the transmittance of thin cross shaped metal meshes with geometrical parameters g = 24 μm, 2a = 9.6 μm, 2b = 3.6 μm, metal thickness of 0.2 μm and surface impedance of 1.635 Ohm cm. The calculated transmittance is shown in Fig.3 with resonance wavelength λ_R = 32.8 μm.
The resonance wavelength agrees very well with the empirical formula[5]

$$\lambda_R = 2g - 4a + 2b \qquad (10)$$

Using the above values of g, a and b one obtains λ_R = 32.4 μm. The validity of this formula for slightly different values of a and b and a constant g may be seen from Table 1. The formula is not valid for a/g values around 0.2 and b/g values around 0.5 to 1.

B. Bandwidth of a single mesh.

We have studied the dependence of the bandwidth on the cross parameters 2a and 2b for a constant value of g. The transmittance is shown in Fig.3 for five different sets of a/g and b/g. The bandwidth BW is taken as the width at half height divided by the peak wavelength. The BW and peak intensity depending on the pair of values of a/g and b/g are listed in Tab.1

Table 1
Bandwidth depending on a/g and b/g

All g = 24			Peak WL	Peak WL		
# in Fig.3	a/g	b/g	2g-4a+2b	From Fig.3	BW	Intensity
1	0.233	0.008	26	31.5	0.07	0.86
2	0.217	0.042	29.2	32.8	0.13	0.97
3	0.200	0.075	32.4	32.8	0.18	0.98
4	0.183	0.108	35.6	33.7	0.26	0.99
5	0.133	0.208	45.2	33.2	0.63	1

One finds from Table 1 that a bandwidth of 13% to 18% with a theoretical transmittance close to 1 may be obtained for a/g values of about 0.2 and b/g values of about 0.05. This is in good agreement with the study by Chase and Joseph[5] on the bandwidth of cross shaped metal meshes.

5. Single metal mesh supported by dielectric layers.

A. The "pair of coupled surface plasmons" model.

Ulrich[18] and Popov[19] have given a general analysis of the modes of a 2D periodic metal mesh. The resonance wavelength λ_R, discussed above, corresponds to a resonance frequency of one of these modes. The incident light excites this mode, and the incident energy is transformed to the reflected and transmitted light waves.

A mode of the metal mesh consists of a pair of coupled surface plasmons. When a surface plasmon on one side of the mesh propagates in a dielectric layer, the resulting resonance wavelength of the metal mesh mode will shift to longer wavelength and even more when the metal mesh is embedded in a dielectric.

B. Transmission line theory and experimental data.

Transmission line theory cannot be used to calculate the resonance wavelength and bandwidth of a metal mesh. They are chosen as input parameters related to an electrical resonance circuit. Whitbourn and Compton[13] have analyzed the role the capacitance plays in the electrical circuit with respect to the resonance frequency. They conclude that the resonance frequency is shifted by a factor of $\sqrt{[2/(n_1^2 + n_2^2)]}$, where n_1 is the refractive index on one side of the mesh and n_2 on the other. We have investigated[9] experimentally a thin cross shaped mesh on a Silicon substrate of 500 μm thickness and found λ_R shifted by a factor of 2.48. From the square root expression one has a shift of 2.5 for a dielectric constants of $n_1 = 1$ on one side and $n_2 = 3.4$ (Silicon) on the other side.

C. Inductive metal mesh and dielectric layers.

The Micro-Stripes program has been applied to calculations of the transmittance of cross shaped metal meshes on a substrate or embedded in a dielectric. The parameters of the mesh are g = 20 μm, 2a = 1.5 μm, 2b = 3 μm, and t = 0.2 μm. Calculations were performed for a free standing mesh, a mesh on a substrate of refractive index n = 1.5 and thickness d = 7 μm and embedded in a dielectric, with thickness of 7 μm on each side. The results are shown in Fig.4. The shift of the resonance wavelength of the metal mesh on the substrate of refractive index n = 1.5 is 9.1 μm (22.8%), and for the embedded case 20.6 μm (51.6%).

D. Wavelength dependence of the resonance mode on the thickness of the dielectric layers and the extent of the surface plamons in the normal direction.

The amplitudes of the surface plasmons on both sides of the metal mesh surface have an exponential decrease in the z-direction, that is the direction perpendicular to the surface, see Ref.20. The resonance wavelength shifts depending on the thickness of the dielectric layer. At zero thickness the resonance wavelength is the same as for a free standing mesh. With increasing thickness the resonance wavelengths shifts to longer wavelength. After the thickness has reached a value corresponding to a sufficient decrease of the amplitude in z-direction, the resonance wavelength does not shift any more.
The Micro-Stripes program has been used to calculate the resonance wavelength depending on thickness of a dielectric substrate of refractive indices 1.5, 2.4 and 3.4, see Fig. 5. The parameters of the mesh are g = 20 μm, 2a = 1.5 μm, 2b = 3 μm, and t = 0.2 μm and substrate thickness of 0 to 18 μm. The resonance wavelength shifts to longer wavelength for all three refractive indices. The shift, after a first maximum, becomes smaller. This is attributed to interaction of the resonance modes with an internal

reflection mode of the plane parallel dielectric layer. In Fig.6 we compare the dependence of the resonance wavelength of a metal mesh on a dielectric substrate with a mesh embedded in a dielectric. One mesh is on a substrate of n = 1.5 and thickness d, the other supported on both sides by a dielectric layer of thickness d and again n = 1.5. The shift for the embedded mesh is always larger. It appears from Fig.5 that the extent of the surface plasmons into the z-dielectric is approximately 1/2 of the periodicity constant g divided by the refractive index.

6. Two metal meshes with dielectric spacer or embedded in a dielectric.

A. Micro-Stripes and Transmission line calculations.

The Micro-Stripes program was applied to transmittance calculations of two meshes separated by a dielectric spacer of thickness d, or embedded in a dielectric. The geometrical parameters of the meshes are g = 24 μm, 2a = 9.6 μm, 2b = 3.6 μm and t = 0.2 μm. There are two configurations for the two meshes, one with the openings of the two meshes lined up (A) and the other with the openings of one mesh in the middle between the openings of the other mesh (B) (see Fig.7).
Transmission line theory does not assume any "line up" of the crosses of one mesh with respect to the other and is therefore much closer to experimental set-ups of the two cross shaped meshes. While transmission line calculations do not account for the shift of the resonance wavelength of the mesh depending on the thickness of the dielectric layers, one can qualitatively study the interaction of the modes of the two meshes. We call the modes of the meshes M-modes and for non-zero interaction of the two meshes one has two different resonance wavelengths. The difference gets smaller and smaller with increasing spacing and at a certain distance a new mode appears, and its peak wavelength shifts to longer and longer wavelengths for increasing thickness. We call this mode the FP-mode because of its similarity to the modes of a Fabry-Perot with two reflector plates at distance d.

B. Refractive index n =1.5.

a. Transmission line calculations for d = 2 to 16 μm.

We assume for this qualitative study that there is no dependence of the resonance wavelength on the thickness of the dielectric spacer or layers. The transmittance is calculated for two meshes with spacer and embedded in a dielectric for the range of d = 2 to 16 μm and d* = 10 μm, see Fig.8. The mesh parameters are a1 = .001, A1 = 0.1 and λ_o = 32.4 μm, corresponding to values of g = 24 μm, 2a = 9.6 μm, 2b = 3.6 μm. The peak wavelengths of the lowest calculated peaks are plotted in Fig.8 for both, the case of a spacer (SP) and the embedded case (EM) and for spacers of 4 and 8 μm in Fig.9 to 12 (TLT). For the (SP) and (EM) configuration see Fig.7.

b. Micro-Stripes calculations for spacer of thickness 4 and 8μm.

The transmittance for two meshes, separated by a dielectric spacer of thickness of 4 μm is shown in Fig.9 and for 8 μm in Fig.10.
In Fig.9 we have for filter (A) and (B) 2 M-modes and one FP- mode and 2 M-modes for (TLT).
In Fig.10 we have for filter (A) and (B) 2 M-modes and one FP- mode and 2 M-modes for (TLT). The interaction of the 2 M-modes of (B) and (TLT) decreases, while the interaction of the 2 M-modes of (A) are zero.

c. Embedded with spacers of 4 and 8 μm and layers of 10 μm.

The transmittance for two meshes embedded in a dielectric with thickness d* of "outside dielectric layers" of 10 μm and spacer of thickness of 4 μm is shown in Fig.11 and for 8 μm in Fig.12.
In Fig.11 we have 2 M-modes and one FP- mode for filter (B) and 2 M-modes for (TLT). The M-modes of filter (A) show decrease intensity.
In Fig.12 we have 2 M-modes and one FP- mode for filter (B) and 1 M-modes for (TLT). The interaction of the 2 M-modes of (B) and (TLT) decreases, while the interaction of the 2 M-modes of (A) are zero for increasing distance.

C. Refractive index n =3.4.

a. Transmission line theory of a two coupled oscillator model.

We have calculated the transmittance of two meshes with spacer and embedded in dielectric for d = 2 to 16 μm, d* = 5 μm, and mesh parameters a1 = 0.001, A1 = 0.1 and λ_o = 32.4 μm, corresponding to values of g = 24 μm, 2a = 9.6 μm, 2b = 3.6 μm. Similarly as discussed above we ignore the thickness dependence of the spacer in this approximate calculations. The result of the peak wavelengths of the lowest calculated peaks are plotted in Fig.13 for both, the spacer and the embedded case and also for spacers of 4 and 8 μm in Fig.14 to 17 (TLT).

b. Dielectric spacer of thickness 4 and 8 μm.

The transmittance for two meshes, separated by a dielectric spacer of thickness of 4 μm is shown in Fig.14 and for 8 μm in Fig.15.
In Fig.14 we have 2 M-modes and one FP- mode for filter (A) and (B) and 2 M-modes for (TLT).
In Fig.15 we have 2 M-modes and 2 FP- modes for filter (A) and (B), and 2 M-modes and one FP-mode for (TLT). The interaction of the 2 M-modes of (A), (B) and (TLT) have decreased for larger spacing.

c. Embedded in dielectric with spacer of thickness 4 and 8 μm and layers of 5 μm.

The transmittance for two meshes embedded in a dielectric with thickness d* of "outside dielectric layers" of 5 μm and spacer of thickness of 4 μm is shown in Fig.16 and for 8 μm in Fig.17.
In Fig.16 we have 2 M-modes and one FP- mode for filter (A) and (B) and 2 M-modes for (TLT). The M-modes of filter (A) show decrease intensity.
In Fig.17 we have 2 M-modes and one FP- mode for filter (A) and (B) and 2 M-modes for (TLT). The interaction of the 2 M-modes of (B) and (TLT) have decreased, while the interaction of the 2 M-modes of (A) are zero.

D. Discussion.

From the qualitative study of the modes, see Fig.8 and 13, one expects that the interaction of the modes decreases from spacing of 4 μm to spacing of 8 μm and is smaller for the (EM) case than for the (SP) case. This is shown in Fig.9 to 12 for n = 1.5 and Fig. 14 to 17 for n = 3.4.
The $\lambda/4$ spacing of the two meshes without any dielectrics, that is for two free standing meshes is 8 μm. Fig. 8 and 13 show minimum interaction at that spacing, and less splitting is seen in Fig.9 to 12 and Fig. 14 to 17 for most peaks.
One has smaller interaction of all modes for low refractive index. For n = 1.5, comparing Fig.10 to Fig.12, one sees that the (TLT) modes reduces their interaction such that only one line appears, while for the (EM) case, the filter A configuration reduces the transmittance to a single line.

7. Filter design.

A. Single mesh filter.

a. Calculation of resonance wavelength and bandwidth.

The Micro-Stripes program calculates the resonance wavelength λ_R of a free standing metal mesh depending on g, a, b and metal thickness t. The calculated peak wavelength agrees very well with the empirical formula $\lambda_R = 2g - 4a + 2b$. The resonance wavelength of the metal shifts to longer wavelength when supported by dielectric films. The Micro-Stripes program calculates also the shifted resonance wavelength for given refractive index and thickness of dielectric layers on one side of the mesh or on both.
The dependence of the bandwidth of a single free standing mesh on the choice of the parameters g, a, and b suggest to use for a narrow bandwidth of 15% values of a/g around 0.2 and b/g around 0.05, see Table 1.

B. Two mesh filter.

a. Micro-Stripes calculations of resonance wavelength and bandwidth using the Micro-Stripes program for two mesh filter with dielectrics.

In order to reduce the bandwidth of a single mesh one uses two meshes mounted parallel at distance d. The experimental mounting results usually in a "non-aligned" configuration. The Micro-Stripes program can only calculate the aligned configurations A and B. The configuration A may be used for narrow band pass filters with high transmittance while the configuration B offers a high reduction of short wavelength light, but usually displays more than one resonance peak.

b. Transmission line calculation of bandwidth using transmission line theory for two mesh filter with dielectrics.

Transmission line theory can calculate the transmission of two metal meshes with crosses in the "non-aligned" configuration, but it cannot correctly include the shift of the resonance wavelength originating from the dielectric spacer of thickness d and refractive index n. The percentage shift of the resonance wavelength of the free standing mesh is larger for high refractive index material than for low ones. A choice of Silicon with n = 3.4 results in a large wavelength shift depending on thickness, while a low refractive index of n = 1.5 makes approximate methods useful.
One obtains a small bandwidth when the interaction of the resonance wavelength of the two meshes is small, that is for meshes in free space at a spacing of $\lambda_R/4$. To minimize the interaction between the two meshes separated by a dielectric spacer, the distance between the two meshes should be $d_s = \lambda_F/4$, where λ_F is the resulting resonance wavelength of the mesh in contact with the dielectric layer. For spacers with low refractive index we discuss the approximate case that the thickness of the spacer is so large that the shift of the resonance wavelength depends only on the refractive index of the spacer and not on the thickness. The shifted resonance wavelength of one mesh is then $\lambda_F = n\,\lambda_R$, and therefore $d_s = n\,\lambda_R/4$. The geometrical distance $d = d_s/n = n\lambda_R/4n = \lambda_R/4$. In this approximation we have for the thickness of the spacer the same value as one obtains for free standing meshes. This has been shown in Section 6 for two meshes with dielectric spacer, see Fig.8, 10 and 12 for n = 1.5
In Fig.18 we show the transmittance for two meshes with spacer of thickness 8 μm, for free standing meshes (F), spacer of refractive index n = 1.5 (SP) and embedded in dielectrics of n = 1.5 (EM), with outside layers of 10 μm. The bandwidth of (F) is 10%, of (EM) is 10% and of (SP) is 12%. One observes that the resonance wavelength is shifted when using dielectric layers, but that the bandwidth remains about the same. altered.

C. Results of Filter design

The resonance wavelength and bandwidth of a single mesh may be calculated from the geometrical parameters of the metal and the supporting films and the loss parameter of the metal and dielectrics.
The resonance wavelength and bandwidth of two metal meshes separated by a dielectric spacer can only be calculated by the Micro-Stripes program for two specific cases of alignment of the crosses of one mesh with respect to the other.
Transmission line theory cannot calculate the resonance wavelength and bandwidth of two metal meshes separated by a dielectric spacer because it does not account for the shift of the resonance wavelength depending on the thickness of the spacer.
An approximate procedure may be used for a dielectric spacer of low refractive index and thickness so large that the dependence on the thickness of the resonance wavelength may be disregarded.

8. Summary.

We have studied the resonance wavelength of cross shaped metal meshes in contact with dielectric layers. The resonance modes of the metal meshes were described by a pair of tightly bound surface plasmons. The dependence of the shift of the resonance wavelength on thickness and refractive index of the dielectric layer was used for an estimate of the width of the surface plasmons in direction perpendicular to the surface of the metal mesh. The resonance wavelength and bandwidth of a single mesh in contact with dielectric layers was calculated using as input data the geometrical parameters, the surface impedance of the metal and the refractive index of the layers.
Using Micro-Stripes calculations, the resonance wavelength of two metal meshes can only be obtained for two specific alignments of the crosses of the meshes with respect to one another. The resonance wavelength of two metal meshes with non-aligned crosses can be calculated approximately for low refractive index materials using transmission line theory.

Acknowledgement

This work was supported by the National Science Foundation, grant number ECS-9820200, and the Naval Research Laboratory.

References

1. R. Ulrich, K. F. Renk, and L. Genzel, IEEE Trans. **MTT-11**, 363 (1963).
2. R. Ulrich, Infrared Phys.7, 37 (1967).
3. G. M. Ressler and K. D. Möller, Appl.Opt. **6**, 893 (1967).
4. R. Ulrich, Infrared Phys.7, 1987 (1967).
5. S. T. Chase and R. D. Joseph, Appl.Opt. **22**, 1775 (1983).
6. T. Timusk and P. L. Richards, Appl.Opt. **20**, 1355 (1981)
7. "Basic Theory of Waveguide Functions and Introductory Microwave Network Analysis" by D. M. Kearns and R. W. Beatty, Pergamon, Oxford,1967.
8. B. C. Hicks, M. Rebbert, P. Isaacson, D. Ma, C. Marrian, J. Fischer, H. A. Smith, P. Ade, R. Sudiwala, M. Greenhouse, H. Moseley, and Ken Stewart. NASA Space Science Workshop, Harvard-Smithsonian Center for Astrophysics, April 1998.
9. K. D. Möller, K. R. Farmer, D. V. P. Ivanov, O. Sternberg, K. P. Stewart, and P. Lalanne, Infrared Physics, **40**,475 (1999).
10. "Micro-Stripes Program" by Flomerics, Inc., 275 Turnpike Road, Suite 100, Southborough, MA 01772.
11. "Near Field Effects in multi-layer Metal Mesh Filters" by K. D. Möller, O. Sternberg, H. Grebel, and K. P. Stewart. To be published.
12. "Far Infrared Spectroscopy" by K. D. Möller and W. G. Rothschild, John Wiley and & Sons, Inc.,1971.
13. L. B. Whitbourn and R. C. Compton, Appl.Opt. **24**, 217 (1985).
14. D. H. Dawes, R. C. McPhedran, and L. B. Whitbourn, Appl.Opt. **28**, 3498 (1989).
15. C. Compton, R. D. McPhedran,G. H. Derrick, and L.C.Bottten, Infrared Phys. **23**, 239 (1983).

16. D. W. Porterfield, J. L. Hesler, R. Densing, E. R. Mueller, T. W. Crowe, and R. M. Weikle II, Appl.Opt.**33**, 6046 (1994).

17. "Hewlett-Packard's" High Frequency Structure Simulator (HFSS).

18. R. Ulrich, Proceedings of the Symposium of Optical and Acoustical Micro-Elecronics, Volume XXIII, New York, NY (1974). Polytechnic Press, Brooklyn NY.

19. E. Popov, M. Neviere, S. Enoch, and R. Reinisch, Phys.Rev.B, 62, 16 100 (2000)

20. "Surface plasmons" by H. Raether, Springer, Berlin,1988.

Figure Captions

Fig.1.
a. Inductive cross shaped mesh, black is metal, bandwidth 40% to 60%..
c. Inductive cross shaped mesh, black is metal, bandwidth 15% to 30%.
c. Geometrical parameters of crosses.

Fig.2.
Shunt impedance with incident and reflected waves on left side with refractive index n_1 and right side with refractive index n_2.

Fig.3.
Bandwidth of cross shaped meshes. The periodicity constant is g = 24 μm. The pairs of a and b values are: (1), a = 5.6 μm and b = 0.2 μm. (2), a = 5.2 μm and b = 1.0 μm. (3), a = 4.8 μm and b = 1.2 μm. (4), a = 4.4 μm and b = 0.26 μm. (5), a = 3.2 μm and b = 5 μm.

Fig.4.
Transmittance of inductive cross shaped metal meshes with g = 20 mμ, 2a = 1.5 mμ, 2b = 3 mμ and thickness 0.2 μm.
a. Free standing, resonance wavelength 39.9 μm.
b. On substrate of thickness 7 μm and refractive index n =1.5, resonance wavelength 49 μm.
c. Embedded in dielectric, thickness of 7 μm on both sides and n = 1.5, resonance wavelength 60.5 μm.

Fig.5
Transmittance of inductive cross shaped metal meshes with g = 20 mμ, 2a = 1.5 mμ, 2b = 3 mμ and thickness 0.2 μm on dielectric substrate of various thickness' and refractive indices. Triangles: n = 3.4, squares n = 2.4, round dots n =1.5.

Fig.6.
Transmittance of inductive cross shaped metal meshes with g = 20 mμ, 2a = 1.5 mμ, 2b = 3 mμ and thickness 0.2 μm and dielectrics of refractive index n = 1.5.
Metal mesh on a substrate (d) and embedded in a dielectric (2d). The embedded metal mesh has a dielectric layer of thickness d on both sides.

Fig.7.
Schematic arrangement of metal mesh and dielectrics. Black lines are metal meshes. Spacer configuration (Sp) with thickness d, Embedded configuration (EM) with d* thickness of layers on "outside" of meshes. In the filter configuration (A) the openings of both metal meshes are "lined up", in configuration (B) the openings of one mesh is in the middle between the openings of the other mesh.

Fig.8.
Transmission line calculations of peak wavelength of two meshes with dielectrics of n = 1.5 depending on thickness of spacer d = 2 to 16 μm. Transmission line parameters λ_o = 32.4 μm, A1 = 0.1, a1 = 0.001 corresponding to g = 24 μm, 2a = 9.6 μm, 2b = 3.6 μm and thickness of 0.2 μm The thickness of the outside layer for the embedded case is d* = 10 μm. Squares (SP): spacer only. Round dots (EM): embedded.

Fig.9. Two metal meshes with spacer of refractive index n = 1.5 and thickness d = 4 μm. Geometrical parameters of g = 24 μm, 2a = 9.6 μm, 2b = 3.6 μm and thickness of 0.2 μm. Shaded line (A): Micro-Stripes calculation of filter. Solid line (B): Micro-Stripes calculation of filter. Broken line: Transmission line theory (TLT) using parameters λ_o = 32.4 μm, A1 = 0.1, a1 = 0.001.

Fig.10. Two metal meshes with spacer of refractive index n = 1.5 and thickness d = 8 μm. Geometrical parameters of g = 24 μm, 2a = 9.6 μm, 2b = 3.6 μm and thickness of 0.2 μm. Shaded line (A): Micro-Stripes calculation of filter. Solid line (B): Micro-Stripes calculation of filter. Broken line: Transmission line theory (TLT) using parameters λ_o = 32.4 μm, A1 = 0.1, a1 = 0.001.

Fig.11. Two metal meshes embedded in a dielectric of refractive index n = 1.5, spacer thickness of d = 4 μm and outside layer of thickness d* = 10 μm. Geometrical parameters of g = 24 μm, 2a = 9.6 μm, 2b = 3.6 μm and thickness of 0.2 μm. Shaded line (A): Micro-Stripes calculation of filter. Solid line (B): Micro-Stripes calculation of filter. Broken line: Transmission line theory (TLT) using parameters λ_o = 32.4 μm, A1 = 0.1, a1 = 0.001.

Fig.12. Two metal meshes embedded in a dielectric of refractive index n = 1.5, spacer thickness of d = 8 μm and outside layer of thickness d* = 10 μm. Geometrical parameters of g = 24 μm, 2a = 9.6 μm, 2b = 3.6 μm and thickness of 0.2 μm. Shaded line (A): Micro-Stripes calculation of filter. Solid line (B): Micro-Stripes calculation of filter. Broken line: Transmission line theory (TLT) using parameters λ_o = 32.4 μm, A1 = 0.1, a1 = 0.001.

Fig.13.
Transmission line calculations of peak wavelength of two meshes with dielectrics of n = 3.4 depending on thickness of spacer d = 2 to 16 μm. Geometrical parameters of g = 24 μm, 2a = 9.6 μm, 2b = 3.6 μm and thickness of 0.2 μm corresponding to transmission line parameters λ_o = 32.4 μm, A1 = 0.1, a1 = 0.001. The thickness of the outside layer for the embedded case is d* = 5 μm. Squares (SP): spacer only. Round dots (EM): embedded.

Fig.14. Two metal meshes with spacer of refractive index n = 3.4 and thickness d = 4 μm. Geometrical parameters of g = 24 μm, 2a = 9.6 μm, 2b = 3.6 μm and thickness of 0.2 μm. Shaded line (A): Micro-Stripes calculation of filter. Solid line (B): Micro-Stripes calculation of filter. Broken line: Transmission line theory (TLT) using parameters λ_o = 32.4 μm, A1 = 0.1, a1 = 0.001.

Fig.15. Two metal meshes with spacer of refractive index n = 3.4 and thickness d = 8 μm. Geometrical parameters of g = 24 μm, 2a = 9.6 μm, 2b = 3.6 μm and thickness of 0.2 μm. Shaded line (A): Micro-Stripes calculation of filter. Solid line (B): Micro-Stripes calculation of filter. Broken line: Transmission line theory (TLT) using parameters λ_o = 32.4 μm, A1 = 0.1, a1 = 0.001.

Fig.16. Two metal meshes embedded in a dielectric of refractive index n = 3.4, spacer thickness of d = 4 μm and outside layer of thickness d* = 5 μm. Geometrical parameters of g = 24 μm, 2a = 9.6 μm, 2b = 3.6 μm and thickness of 0.2 μm. Shaded line (A): Micro-Stripes calculation of filter. Solid line (B): Micro-Stripes calculation of filter. Broken line: Transmission line theory (TLT) using parameters λ_o = 32.4 μm, A1 = 0.1, a1 = 0.001.

Fig.17. Two metal meshes embedded in a dielectric of refractive index n = 3.5, spacer thickness of d = 8 μm and outside layer of thickness d* = 5 μm. Geometrical parameters of g = 24 μm, 2a = 9.6 μm, 2b = 3.6 μm and thickness of 0.2 μm Shaded line (A): Micro-Stripes calculation of filter. Solid line (B): Micro-Stripes calculation of filter. Broken line: Transmission line theory (TLT) using parameters λ_o = 32.4 μm, A1 = 0.1, a1 = 0.001.

Fig.18.
Transmission line calculations of peak wavelength of two meshes of spacer thickness of 8 μm. Transmission line parameters λ_o = 32.4 μm, A1 = 0.1, a1 = 0.001. Free standing meshes (F), spacer of refractive index n = 1.5 (SP) and embedded in dielectrics of refractive index n = 1.5 with d* = 10 μm (EM). The ratio of bandwidth at half height to peak wavelength is for all three about 0.1.

Appendix A

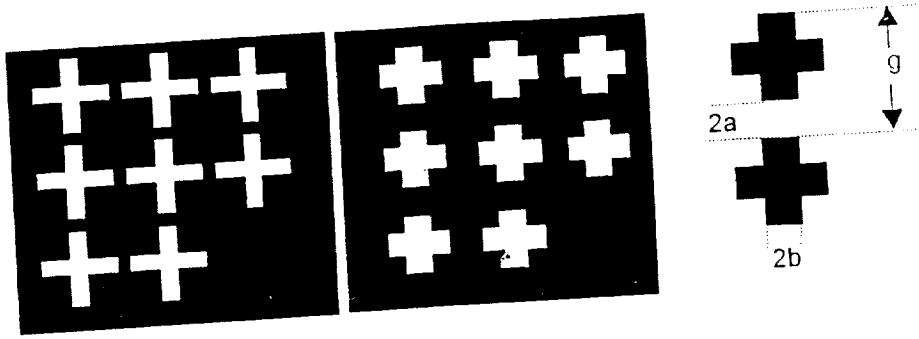

(a) (b) (c)

Fig. 1

Appendix A

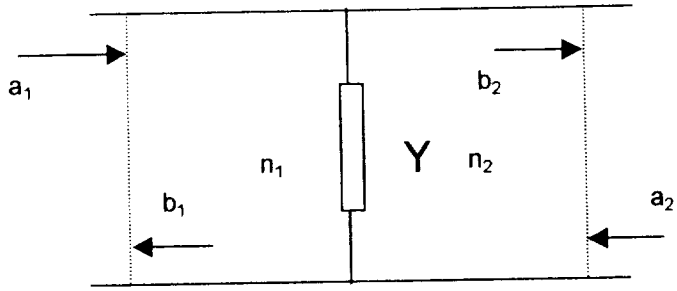

Fig. 2

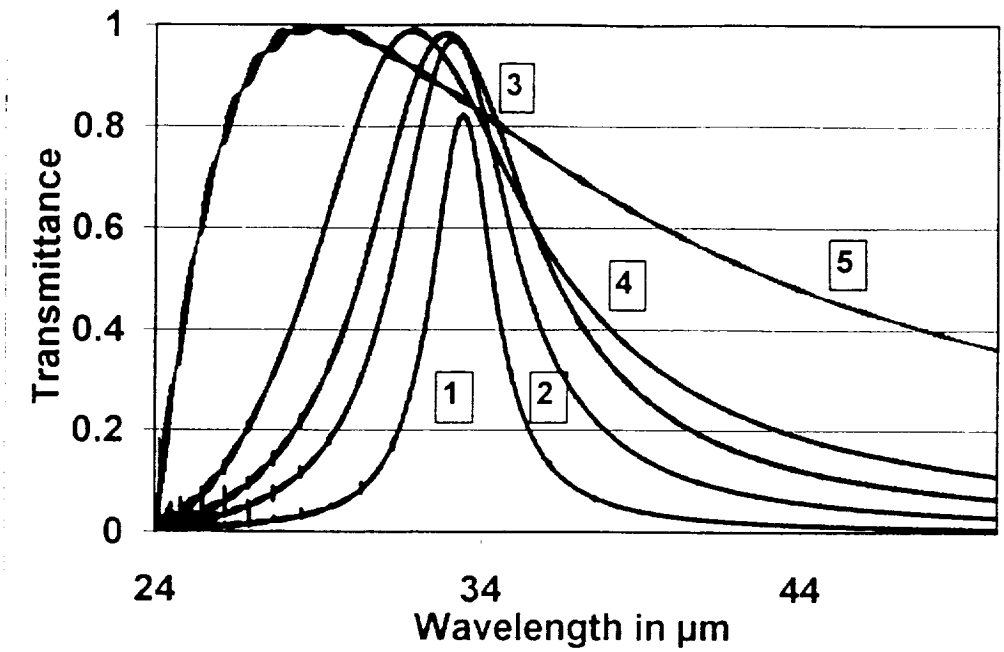

Fig. 3

Appendix A

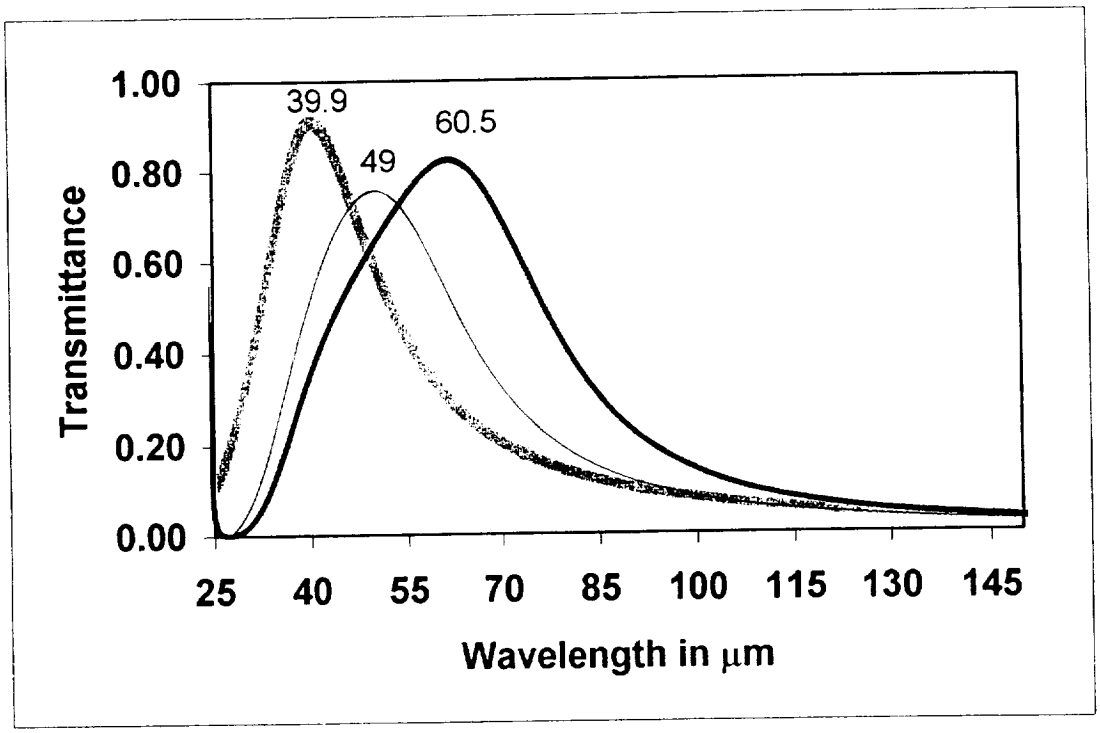

Fig. 4

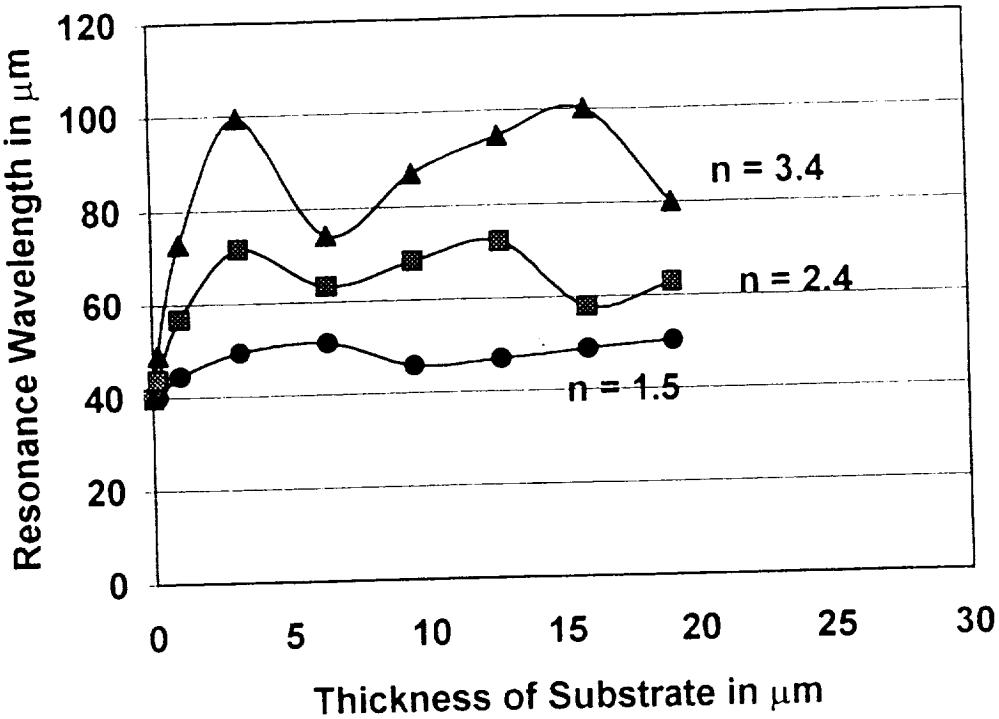
Resonance Wavelength in μm
120
100
80
60
40
20
0
0
5
10
15
20
25
30
Thickness of Substrate in μm
n = 3.4
n = 2.4
n = 1.5

Fig. 5

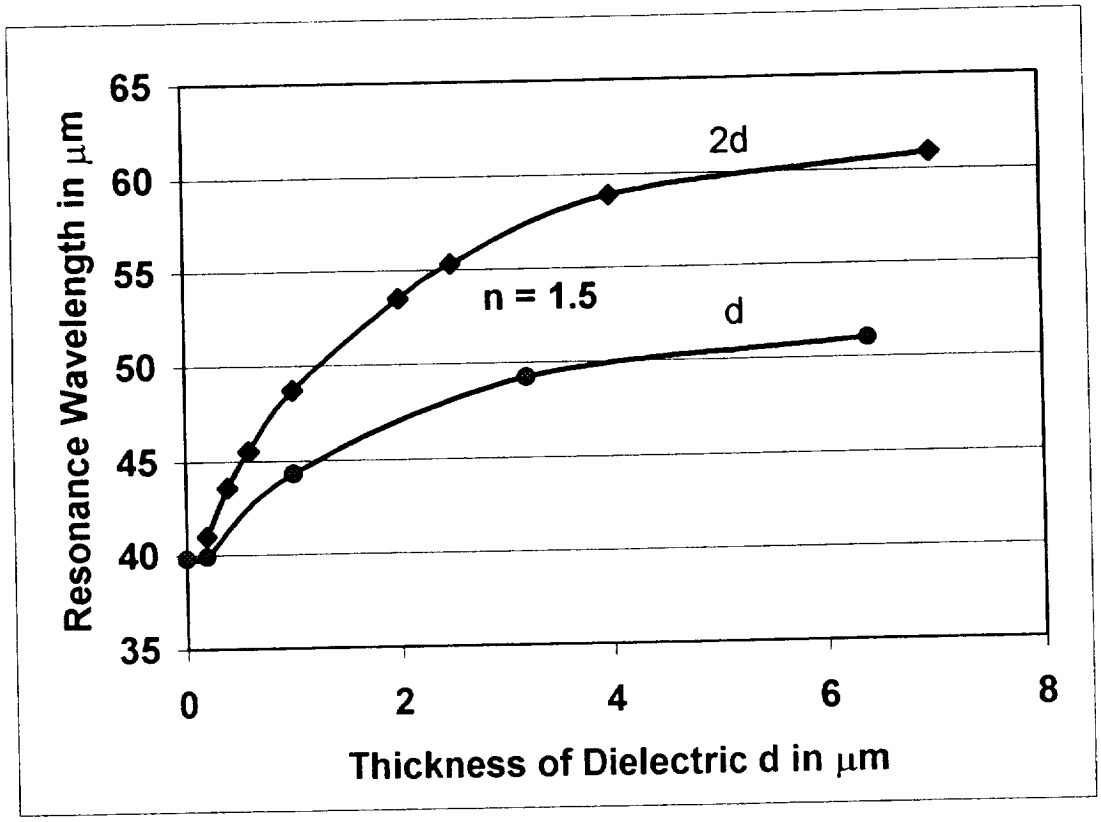
Resonance Wavelength in μm
65
60
55
50
45
40
35
0
2
4
6
8
Thickness of Dielectric d in μm
2d
n = 1.5
d

Fig. 6

Appendix A

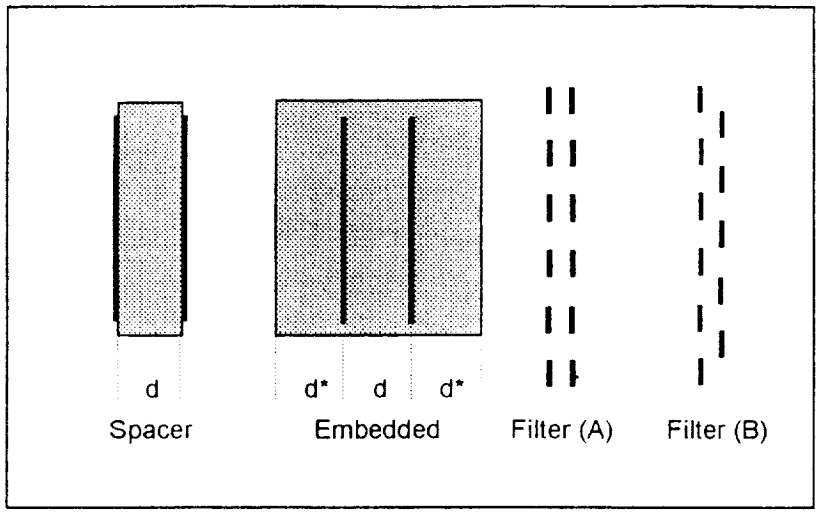

Fig. 7

Appendix A

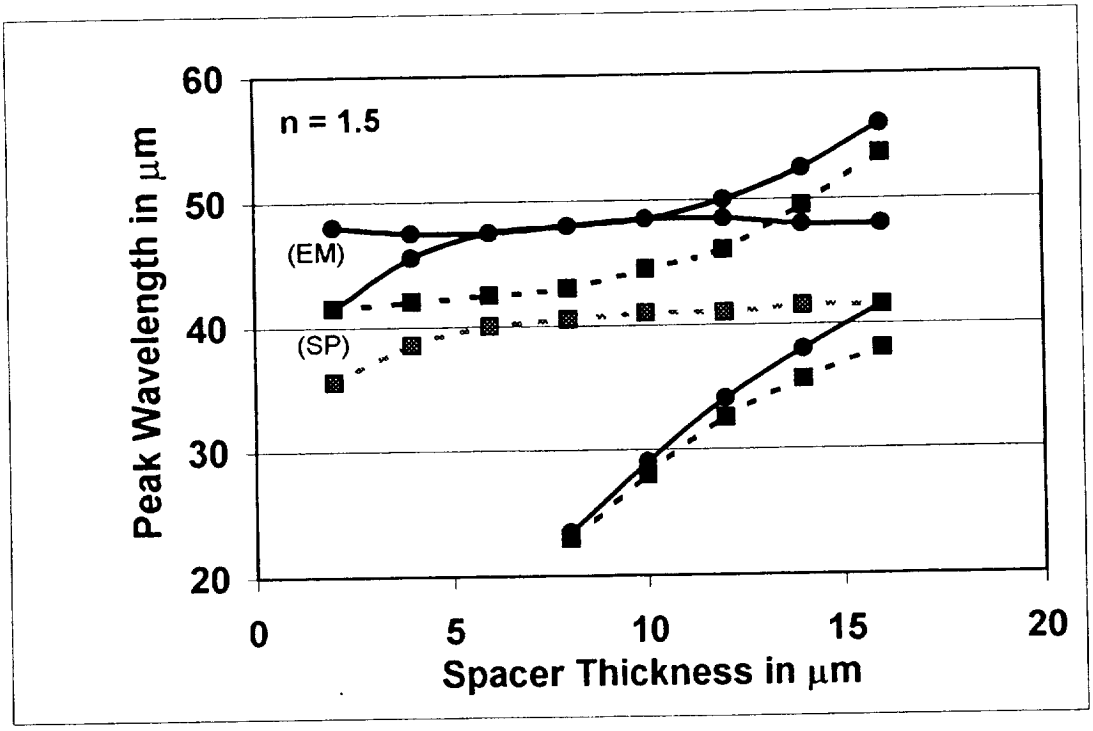

Fig. 8

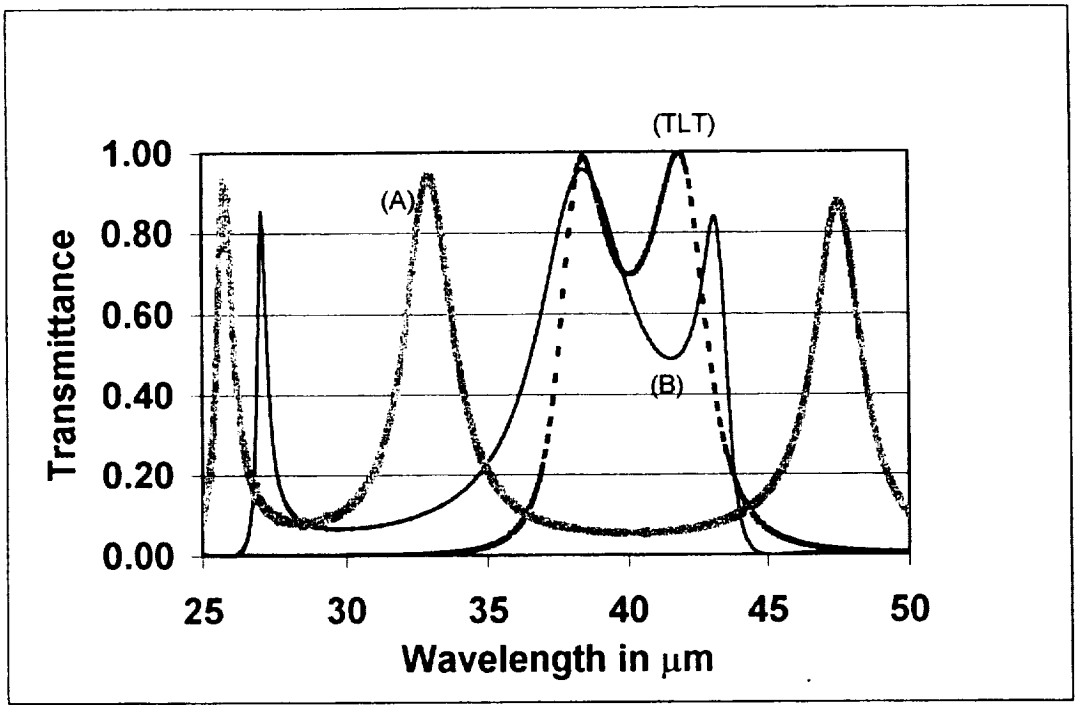
(TLT)
(A)
(B)
1.00
0.80
0.60
0.40
0.20
0.00
Transmittance
25
30
35
40
45
50
Wavelength in μm

Fig. 9

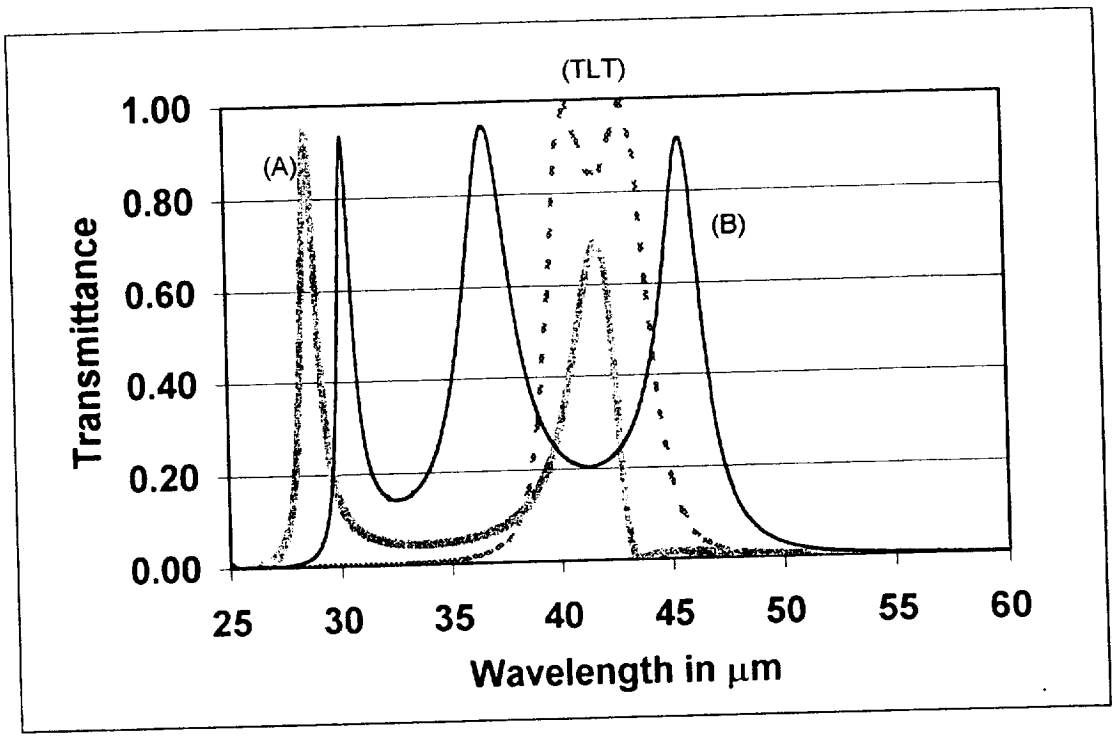
(TLT)
1.00
0.80
0.60
0.40
0.20
0.00
Transmittance
(A)
(B)
25
30
35
40
45
50
55
60
Wavelength in μm

Fig. 10

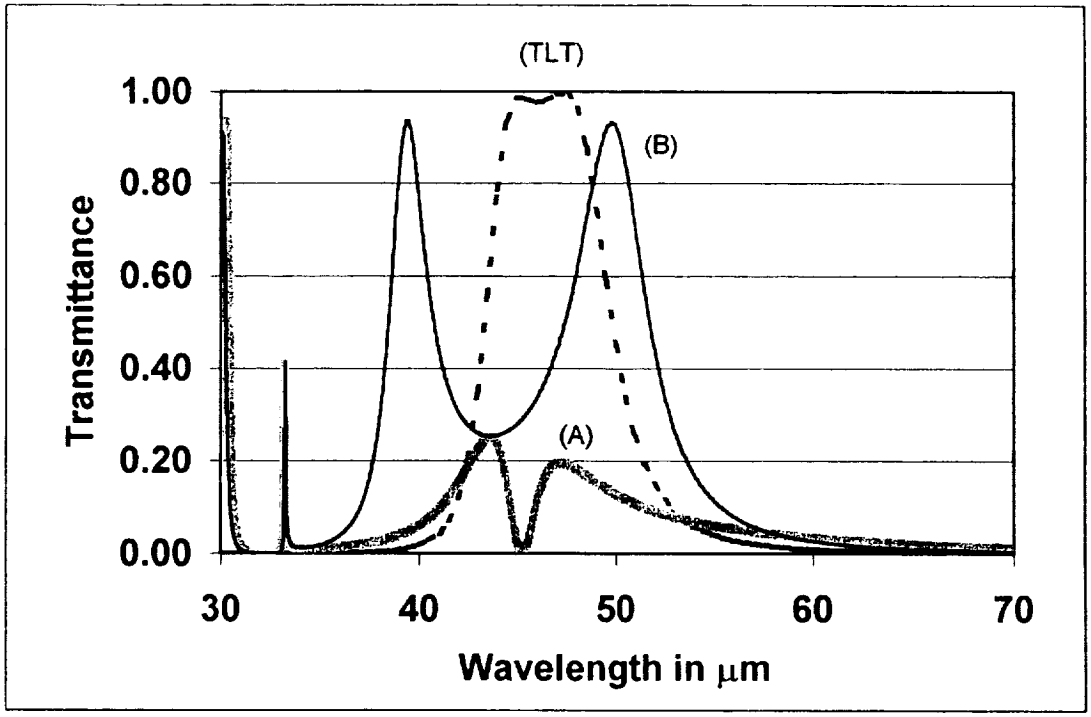
(TLT)
1.00
0.80
0.60
0.40
0.20
0.00
Transmittance
(B)
(A)
30
40
50
60
70
Wavelength in μm

Fig. 11

Appendix A

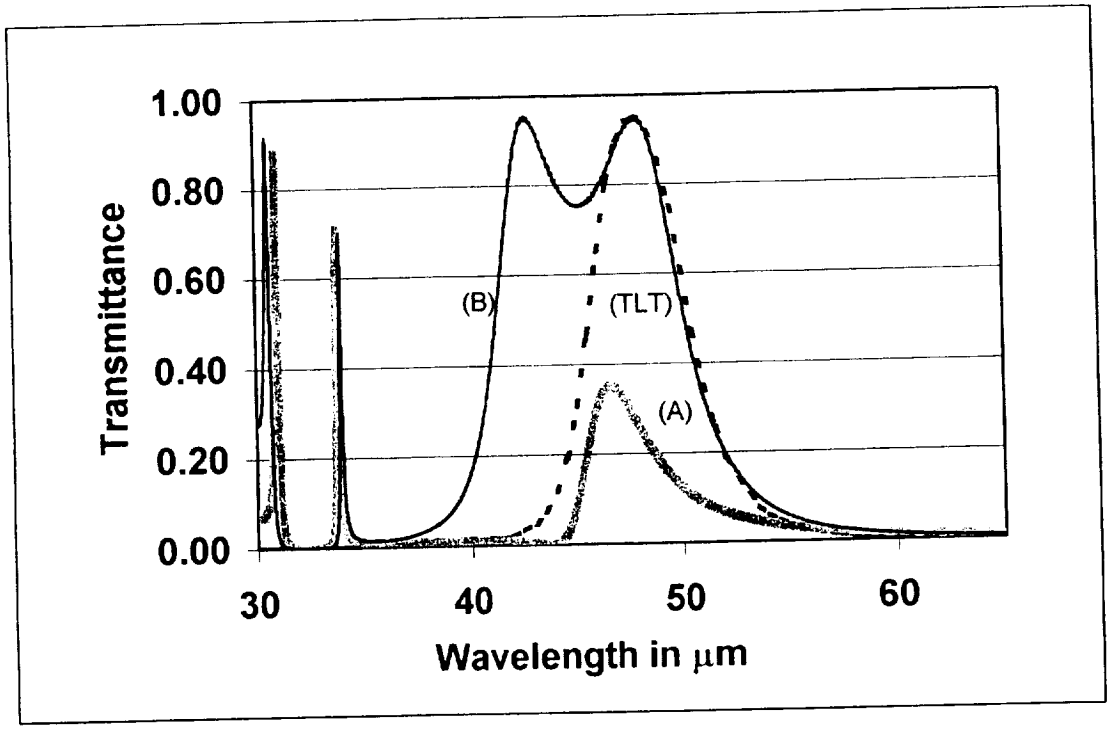

Fig. 12

Appendix A

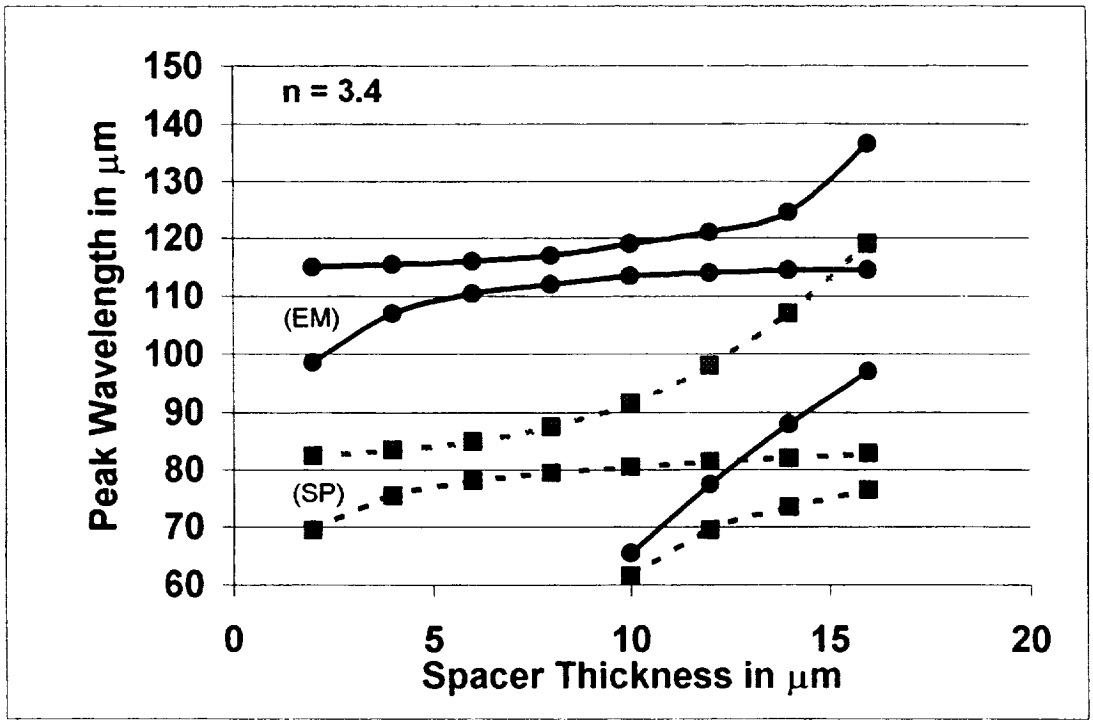

Fig. 13

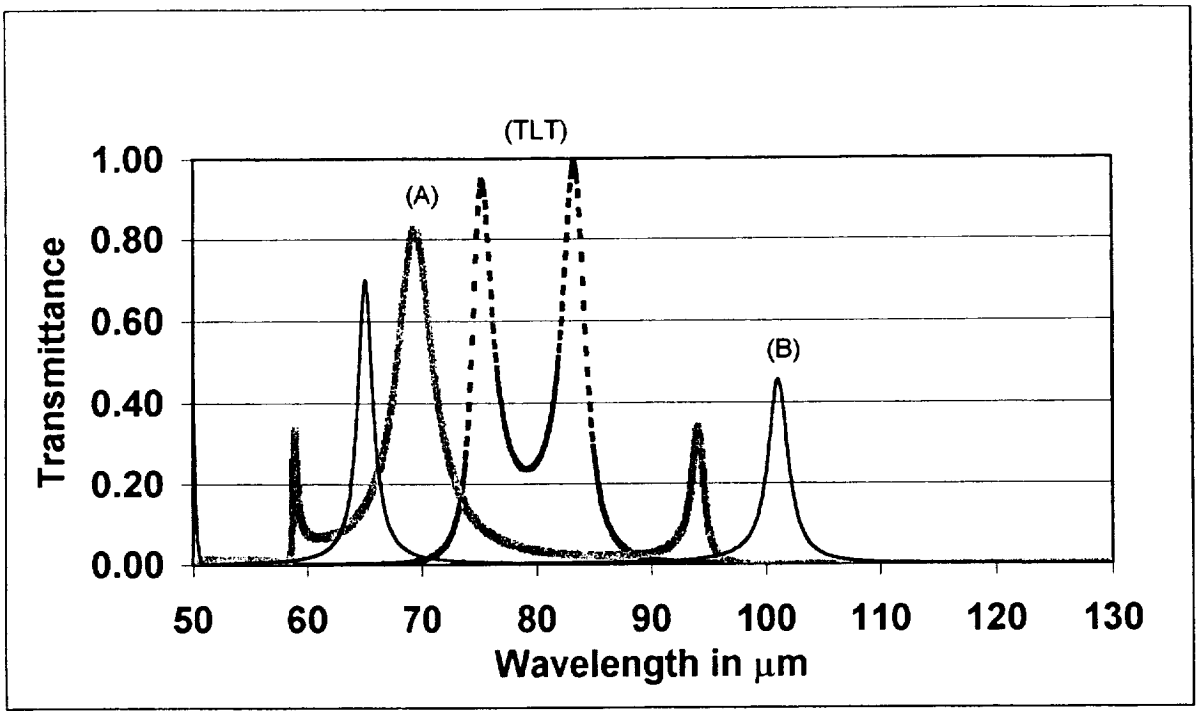
(TLT)
(A)
(B)
1.00
0.80
0.60
0.40
0.20
0.00
Transmittance
50
60
70
80
90
100
110
120
130
Wavelength in μm

Fig. 14

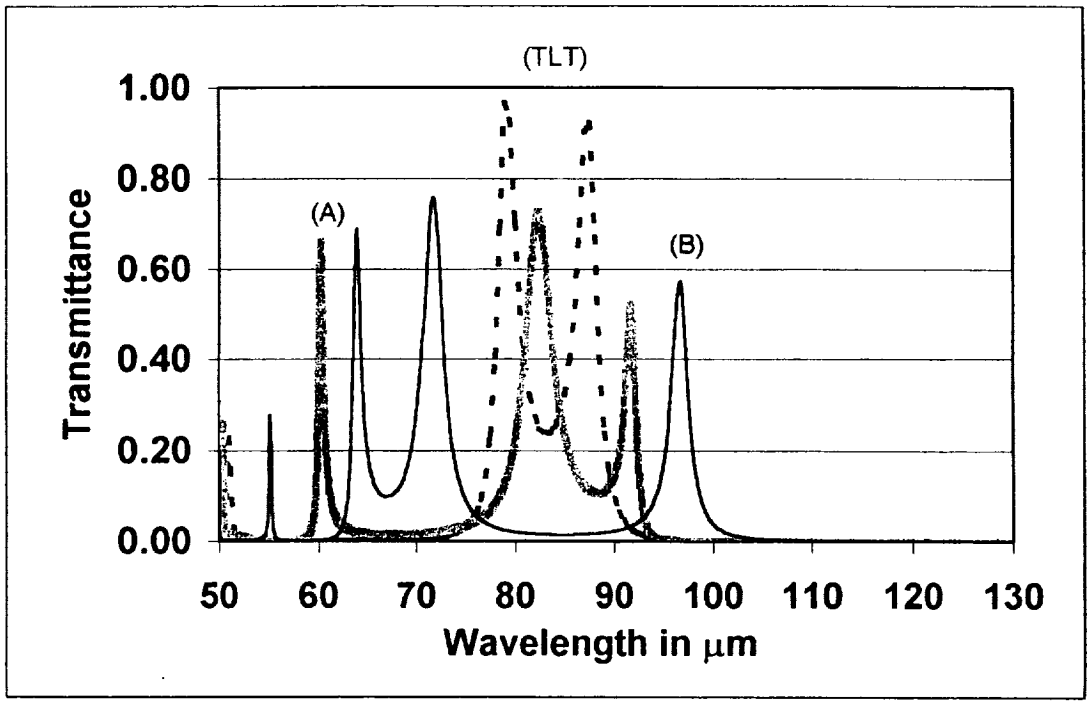
(TLT)
1.00
0.80
0.60
0.40
0.20
0.00
Transmittance
(A)
(B)
50
60
70
80
90
100
110
120
130
Wavelength in μm

Fig. 15

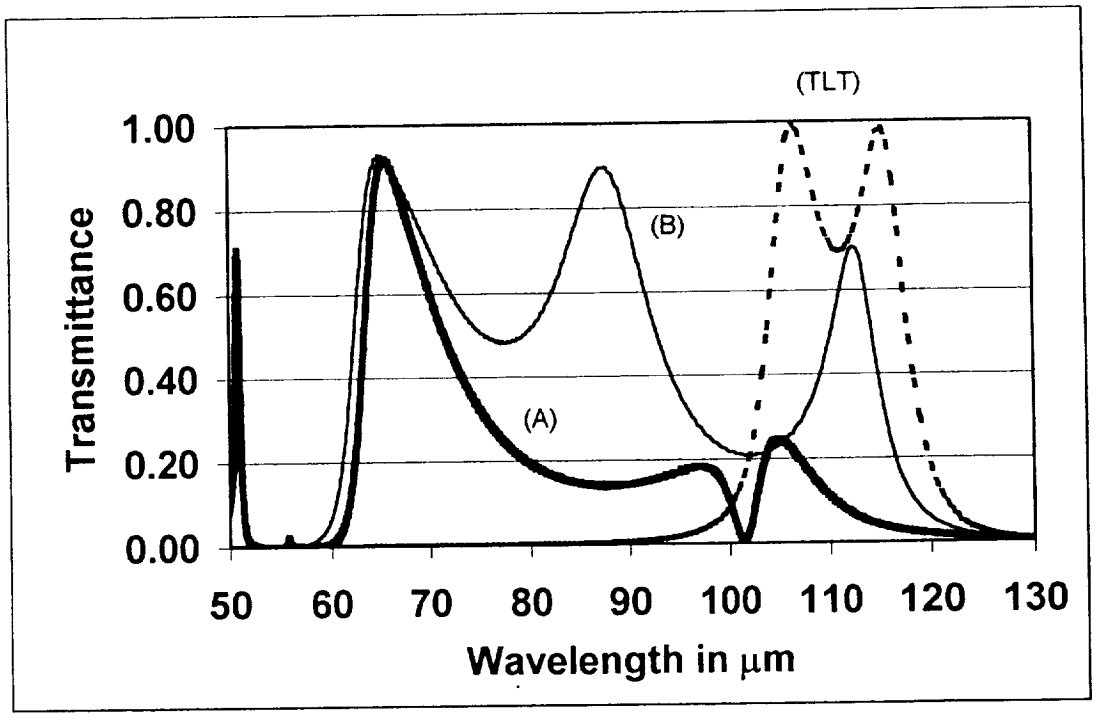
(TLT)
1.00
0.80
0.60
0.40
0.20
0.00
Transmittance
(B)
(A)
50
60
70
80
90
100
110
120
130
Wavelength in μm

Fig. 16

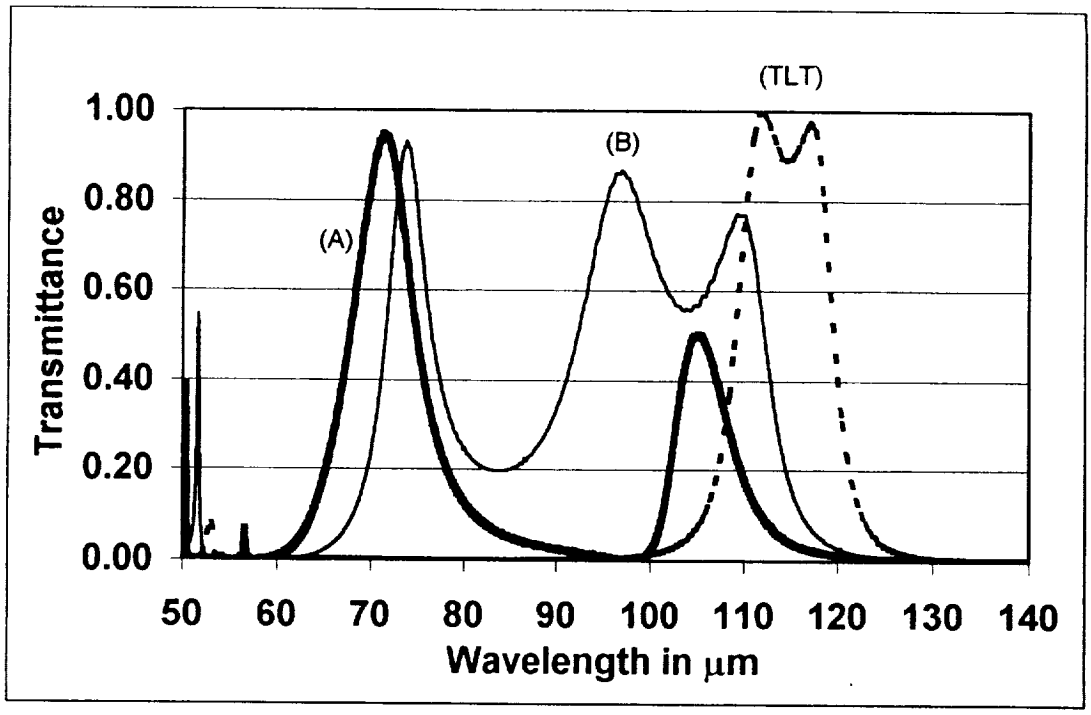
(TLT)
(B)
(A)
1.00
0.80
0.60
0.40
0.20
0.00
Transmittance
50
60
70
80
90
100
110
120
130
140
Wavelength in μm

Fig. 17

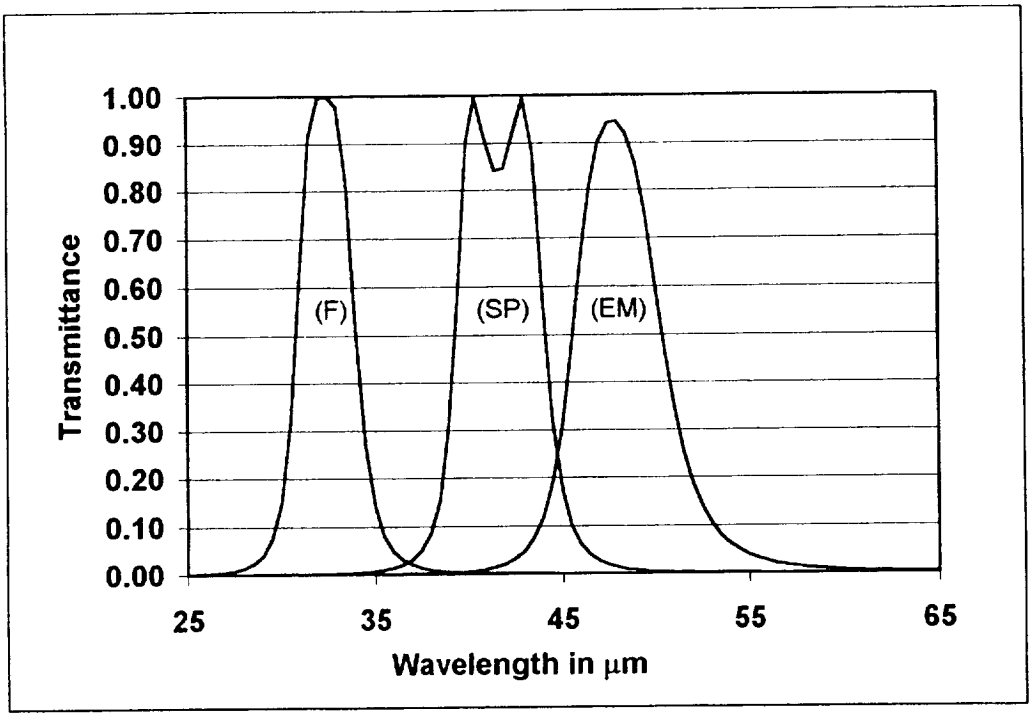
1.00
0.90
0.80
0.70
0.60
0.50
0.40
0.30
0.20
0.10
0.00
Transmittance
(F)
(SP)
(EM)
25
35
45
55
65
Wavelength in μm

Fig. 18

Appendix B

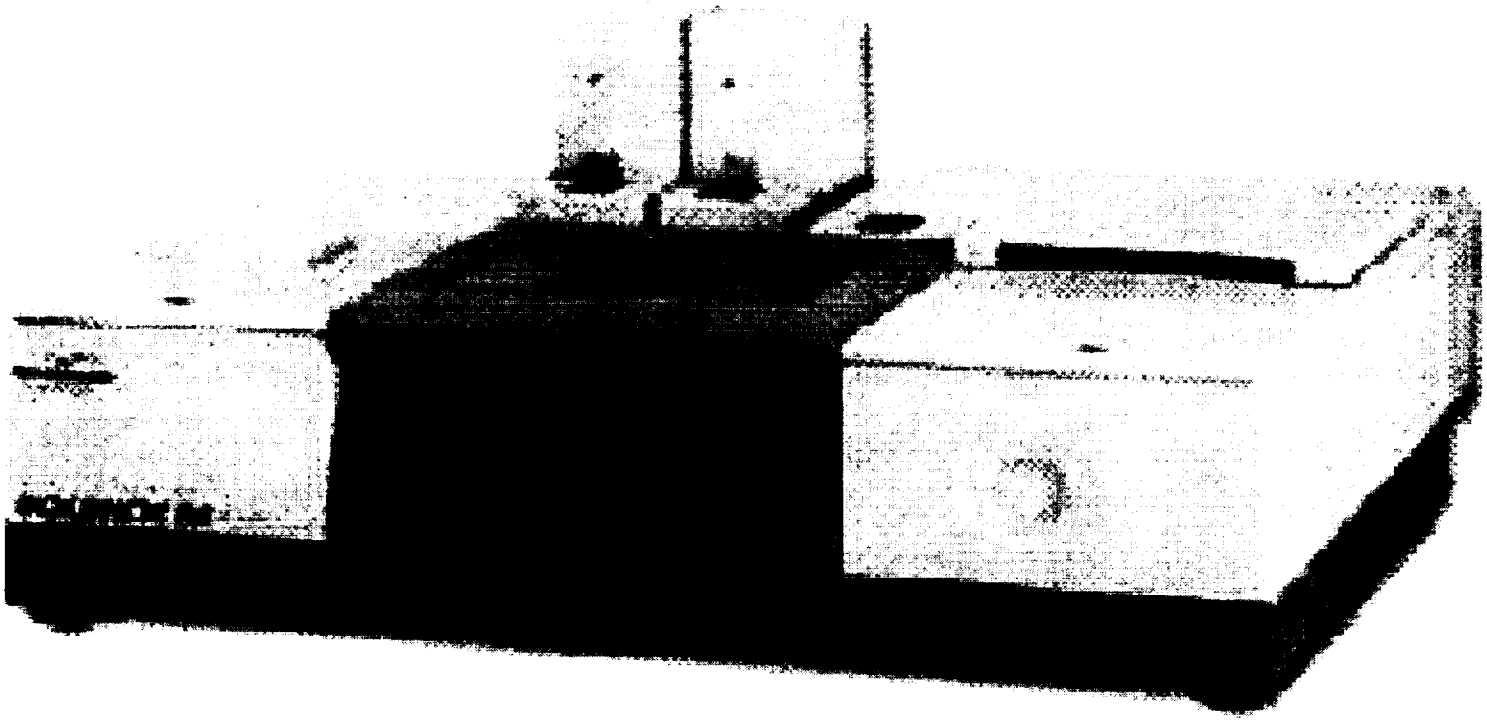

TENSOR[tm] series
FT-IR Spectrometer

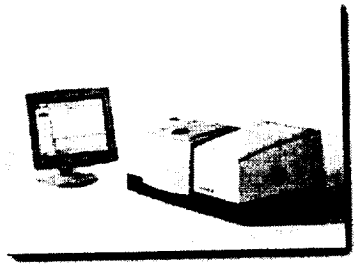

The TENSOR[tm] series is designed to meet the demands of today's and tomorrow's analytical laboratories. It combines the highest performance and outstanding flexibility with an intuitive and easy to operate interface.

Bruker Optics announces the new TENSOR[tm] series , an FT-IR spectrometer designed to meet the demands of today's and tomorrow's analytical laboratories. It combines the highest performance and outstanding flexibility with an intuitive and easy to operate interface.

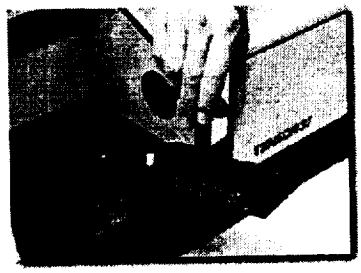

With the new DigiTect[tm] detector system, TENSOR[tm] provides highest sensitivity performance. Permanently aligned, high throughput RockSolid[tm] interferometer ensures stability and durability.

A full line of sampling and automation accessories is available to fulfill the need to expand TENSOR[tm] series.

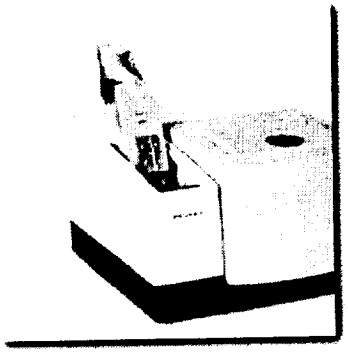

Changing the pre-aligned detector

A network of intelligent features makes FT-IR spectroscopy easy, fast and reliable. Specific software tools complete this outstanding functionality. Online PerformanceGuard[tm] is the insurance for accurate results. All optical components, automation units and accessories of TENSOR[tm] are monitored continuously.

The TENSOR[tm] series are equipped with automatic accessory and automatic component recognition systems.

When an accessory is placed in the sample compartment the accessory will be instantly and automatically recognized and tested. All relevant parameters transferred to the software, so that you can immediately start your measurements.

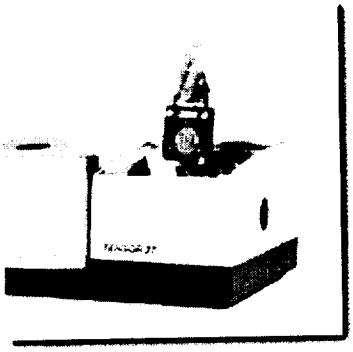

Beamsplitter change

All optical components like source, detector, beamsplitter, and laser can easily be changed and are recognized by the IntelliSense[tm] coding. Even untrained personnel can exchange components or expand the wavelength range to NIR (TENSOR[tm] 37).

RESEARCH

The Fastest FTIR on Earth . . .

Collect more than 100 spectra per second!

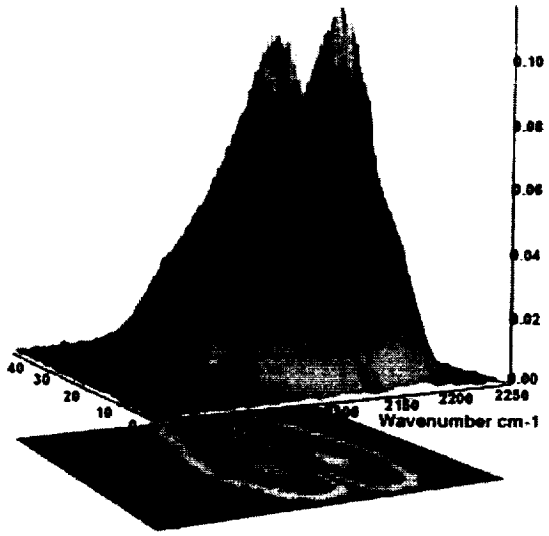

Rapid-scan spectrum of injection of carbon monoxide (CO) demonstrating 20 spectra/second at 2 cm-1 spectral resolution. Shown are the 3-D stack plot (above) and the contour plot (below).

Take a look at these features

- **Flexible triggering options - user selectable master/slave electronics**
- **Linearized detector response**
- **Gain switch at all velocities**
- **Velocities up to 320 kHz (10.1 cm/sec)**
- **Unmatched experimental flexibility via customized macros**

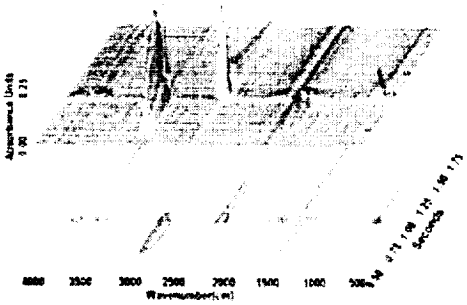

Combustion spectrum from a butane lighter, 8 cm^{-1} resolution, 10 millisecond time resolution.

Guaranteed Spectral Acquisition Rates

IFS 66/S	
RESOLUTION	***ACQUISTION RATE***
16 cm^{-1}	109 spectra / second
12 cm^{-1}	100 spectra / second
8 cm^{-1}	83 spectra / second
4 cm^{-1}	57 spectra / second
2 cm^{-1}	35 spectra / second

EQUINOX 55	
RESOLUTION	***ACQUISTION RATE***
16 cm^{-1}	75 spectra /second
12 cm^{-1}	70 spectra /second
8 cm^{-1}	60 spectra /second
4 cm^{-1}	40 spectra /second
2 cm^{-1}	20 spectra /second

Bruker... A Step Ahead

Bruker introduced step-scan on their FTIR instruments in 1987 and has continued to be a leader in step-scan technology.

- ★ 1988 R&D award winner for the developing the step-scan technique
- ★ Flexible triggering -- user defined master/slave
- ★ Full range of hardware and software for phase- and time-resolved experiments.
- ★ Time-resolved experiments to the picosecond range!
- ★ Phase resolved experiments with amplitudes to ± 25 lamda and frequencies to 1500Hz
- ★ Technical support to ensure your success

Phase Resolved Step-Scan

Time Resolved step-scan

RESEARCH

FIR to the Edge of the Microwave

Bruker offers superior performance in the FIR. Here's why:

- **Evacuated systems**
- **Wide range beamspitters**
- **Down to 4cm^{-1} with Bolometer option**
- **Mercury source available**
- **Over 25 years of experience with FIR spectroscopy**

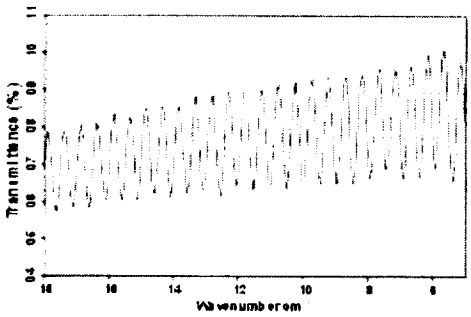

Far-IR transmittance of a 5 mm infrasil filter using étalon fringing to determine filter thickness.

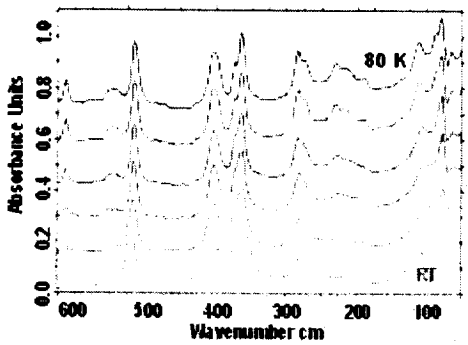

FIR measurements of liquid DMTF at various temperatures. The sample was housed in a CF 1104 cryostat with PE windows. Resolution= 4cm^{-1}, 30 scans, HG-arc source, DTGS-PE detector.

Spectral Range · Polarization Experiments · Raman · Step-Scan · Rapid-Scan · Advantages of Vacuum

FIR MIR NIR

RESEARCH Spectral Range

MIR

Today's beamplitter technology extends the traditional MIR range into the NIR. A single beamsplitter can cover the range from 10,000 to 400 cm^{-1}, providing a cost and time saving way of covering multiple ranges.

Advantages

- **Simultaneous measurement of fundamentals and overtones**
- **Cost saving; one beamsplitter 2 ranges**
- **Fast range change, no disruption of the instrument environment**

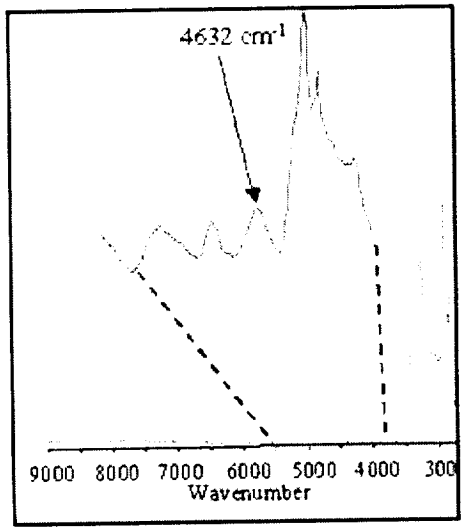

Multi-range chemical image of Rat liver tissure

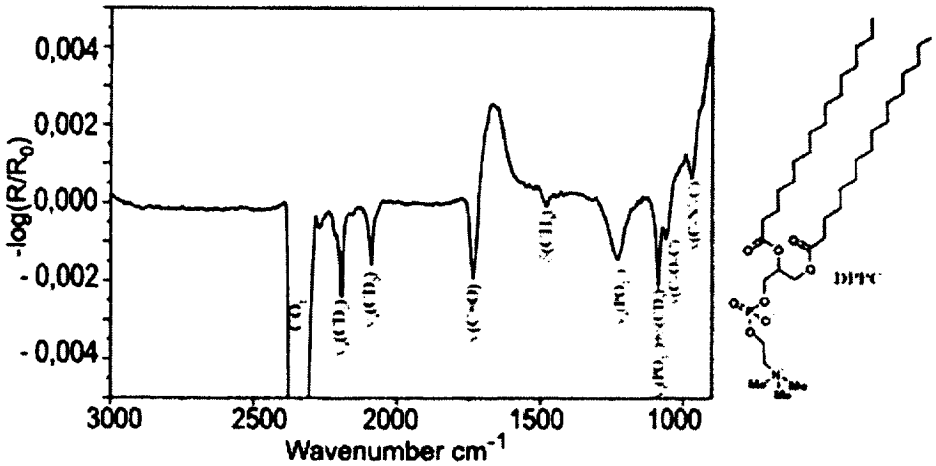

Spectrum of a dipalmitoylphosphatidylcholine monolayer at the air/water interface (DPPC-d62, acyl chains deuterated). Surface pressure 45 mN/m, T = 21°C, pH 5.6, 35° angle of incidence, s-polarization, 4 cm^{-1} resolution, 5 min recording time. The spectrum is shown as obtained, i.e., no smoothing or baseline correction was applied.
